

**GAS SORPTION IN 3,5-DIAMINOBENZOIC ACID (DABA) BASED
POLYIMIDES**

**M.Sc. Thesis by
Işıl KABACAOĞLU**

Department : Chemical Engineering

Programme : Chemical Engineering

Thesis Supervisor: Assoc. Prof. M. Göktuğ AHUNBAY

JUNE 2011

**GAS SORPTION IN 3,5-DIAMINOBENZOIC ACID (DABA) BASED
POLYIMIDES**

**M.Sc. Thesis by
Işıl KABACAOĞLU
506081035**

**Date of submission : 06 May 2011
Date of defence examination: 02 June 2011**

**Supervisor (Chairman) : Assoc. Prof. M. Göktuğ AHUNBAY
(ITU)
Members of the Examining Committee : Prof. Dr. Birgül TANTEKİN-
ERSOLMAZ (ITU)
Assis. Prof. Dr. Aylin KONUKLAR
(ITU)**

JUNE 2011

İSTANBUL TEKNİK ÜNİVERSİTESİ ★ FEN BİLİMLERİ ENSTİTÜSÜ

**3,5-DİAMİNOBENZOİK ASİT (DABA) BAZLI POLİİMİDLERDE GAZ
SORPSİYONU**

**YÜKSEK LİSANS TEZİ
Işıl KABACAOĞLU
506081035**

**Tezin Enstitüye Verildiği Tarih : 06 Mayıs 2011
Tezin Savunulduğu Tarih : 02 Haziran 2011**

**Tez Danışmanı : Doç. Dr. M. Göktuğ AHUNBAY (İTÜ)
Diğer Jüri Üyeleri : Prof. Dr. Birgül TANTEKİN-ERSOLMAZ
(İTÜ)
Yrd. Doç. Dr. Aylin KONUKLAR (İTÜ)**

HAZİRAN 2011

FOREWORD

I would like to thank all of those people who have made remarkable endeavor with me throughout my graduate education.

I would like to express my greatest thanks to my advisor, Dr. M. Göktuğ Ahunbay, who made this thesis possible with his valuable help, support and supervision.

I also would like to extend my deep appreciation to Dr. Birgül Tantekin-Ersolmaz due to her guidance in my experimental studies. I am grateful for the opportunity to being a member of her research group.

Although her 19 inch widescreen PC monitor made me green with envy throughout my computer-aided simulation studies, my very special and sincere thanks go to Sadiye Halitoğlu-Velioğlu for her valuable help and suggestions, friendship and interminable patience all along my graduate studies.

I appreciate Dr. Çiğdem Atalay-Oral and Işık Yavuz who supported my experimental works and analyses with their broad experiences.

In addition, I preciously thank to my supportive lab mates Aylin Kertik, Göktuğ Altay, Selda Şen and Duygu Kahraman for their incontrovertible help.

Last but not least, I offer my intense and greatest thanks to my beloved parents, Yıldız and Kaya Kabacaoğlu for their infinite love and support throughout my life. As Albert Einstein said; “I try not to become a man of success but rather try to become a man of value”, in order to be worthy of them. My kind thanks go to my sisters, Elif and Dilşad, and our mischievous doggy Maya due to their friendship.

May 2011

Işıl Kabacaoğlu

Chemical Engineer

TABLE OF CONTENTS

	<u>Page</u>
ABBREVIATIONS	ix
LIST OF TABLES	xi
LIST OF FIGURES	xiii
ABSTRACT	xv
ÖZET	xvii
1. INTRODUCTION	1
2. THEORY AND BACKGROUND	3
2.1 Gas Transport Mechanism Through Membranes.....	3
2.2 Polyimide Membranes for Gas Separation Applications	5
2.2.1 Free volume in polyimides.....	5
2.2.2 Gas transport in glassy polyimides	6
2.2.3 Plasticization in polyimides	8
2.3 Review of Structure-Solubility Relationship in Polyimides	9
3. MOLECULAR SIMULATION METHODS	11
3.1 Statistical Ensembles	11
3.2 Molecular Forcefields.....	12
3.3 Molecular Dynamics Methods	16
3.4 Monte Carlo Methods.....	19
4. SIMULATION STUDY	21
4.1 System	21
4.2 Methodology	22
4.2.1 Construction and characterization of polyimide matrices.....	22
4.2.2 Sorption in polyimide matrices	25
5. EXPERIMENTAL STUDY	29
5.1 Materials.....	29
5.2 Monomer Purification	30
5.3 Polyimide Synthesis	31
5.4 Characterization of Polyimide.....	34
5.4.1 Fourier transform infrared spectroscopy (FTIR)	34
5.4.2 Thermal gravimetric analysis (TGA).....	34
5.4.3 Differential scanning calorimetry (DSC).....	35
5.4.4 Wide-angle x-ray diffraction (WA-XRD).....	35
6. RESULTS AND DISCUSSION	37
6.1 Simulation Results.....	37
6.1.1 Characterization results.....	37
6.1.2 Sorption results	43
6.2 Experimental Results.....	60
7. CONCLUSIONS AND RECOMMENDATIONS	65
REFERENCES	69
APPENDIX	73

CURRICULUM VITAE..... 77

ABBREVIATIONS

6FDA	: 4,4'-(hexafluoroisopropylidene)diphthalic anhydride
BTDA	: 3,3',4,4'-benzophenonetetracarboxylic dianhydride
DABA	: 3,5-diaminobenzoic acid
DAM	: 2,4,6-trimethyl-m-phenyldiamine
ODA	: 4,4'-oxydianiline
NVT	: Canonical ensemble
NVE	: Microcanonical ensemble
NPT	: Isothermal-isobaric ensemble
μVT	: Grand canonical ensemble
GCMC	: Grand canonical Monte Carlo
CHARMM	: Chemistry at HARvard Macromolecular Mechanics
PCFF	: Polymer-Consistent Force Field
CVFF	: Consistent Valence Force Field
GROMACS	: GROningen Machine for Chemical Simulations
COMPASS	: Condensed-phase Optimized Molecular Potentials for Atomistic Simulation Studies
MD	: Molecular Dynamics
MC	: Monte Carlo
CBMC	: Conformational Bias Monte Carlo
PI	: Polyimide
R_g	: Radius of Gyration
CED	: Cohesive Energy Density
FFV	: Fractional Free Volume
T_g	: Glass Transition Temperature
NMP	: 1-Methyl-2-Pyrrolidinone
DCB	: 1,4-Dichlorobenzene
MeOH	: Methanol
FTIR	: Fourier Transform Infrared Spectroscopy
TGA	: Thermal Gravimetric Analysis
DSC	: Differential Scanning Calorimetry
WA-XRD	: Wide-Angle X-Ray Diffraction
RDF	: Radial Distribution Function

LIST OF TABLES

	<u>Page</u>
Table 3.1 : Statistical ensembles	12
Table 5.1 : Properties of the solvents used in the synthesis of polyimide	29
Table 5.2 : Properties of the monomers used in the polyimide synthesis	30
Table 6.1 : Structural properties of 6FDA-DABA, BTDA-DABA and 6FDA/BTDA-DABA.....	40
Table 6.2 : Solubility coefficients and solubility selectivities of O ₂ , N ₂ , CO ₂ and CH ₄	44
Table 6.3 : Solubility coefficients and solubility selectivities of C ₃ H ₆ and C ₃ H ₈ ...	46
Table 6.4 : Fractional free volume of PI matrices after CO ₂ and CO ₂ /CH ₄ sorption.....	46
Table 6.5 : Fractional free volume of PI matrices after C ₃ H ₆ , C ₃ H ₈ and C ₃ H ₆ /C ₃ H ₈ sorption.	47
Table 6.6 : FTIR bands of poly(amic) acid and polyimide of BTDA-DABA with respect to their functional groups.....	61
Table 6.7 : Weight loss of BTDA-DABA.....	63
Table 6.8 : Glass transition temperature and d-spacing values of BTDA-DABA obtained by simulation and experimental study	64

LIST OF FIGURES

	<u>Page</u>
Figure 1.1 : Robeson curve for H ₂ /N ₂ separation application.....	2
Figure 2.1 : Schematic representation of gas separation through a membrane.....	3
Figure 2.2 : Schematic representation of Henry sorption (a), Langmuir sorption (b) and dual-mode sorption (c).	7
Figure 3.1 : Intermolecular and intramolecular interactions.....	13
Figure 4.1 : Structures of monomers used in simulation study.....	21
Figure 4.2 : Polyimide volume as a function of temperature.....	25
Figure 5.1 : Two step condensation reaction for polyimide synthesis.....	32
Figure 5.2 : Equipment set-up for the polyimide synthesis.	33
Figure 6.1 : X-ray patterns of 6FDA-DABA.	38
Figure 6.2 : X-ray patterns of BTDA-DABA.	38
Figure 6.3 : X-ray patterns of polyimides and copolyimide.	39
Figure 6.4 : Volume of PI matrices as a function of temperature (a) 6FDA-DABA (b) BTDA-DABA and (c) 6FDA/BTDA-DABA.	41
Figure 6.5 : Torsion angle distribution of bridging groups of 6FDA-DABA and BTDA-DABA.....	42
Figure 6.6 : Torsion angle distribution of linkage between dianhydrides and diamine of polyimides and copolyimide.....	39
Figure 6.7 : O ₂ and N ₂ sorption isotherms of polyimides and copolyimide at 35°C.....	45
Figure 6.8 : CH ₄ sorption isotherms of polyimides and copolyimide at 35°C.....	45
Figure 6.9 : CO ₂ , propylene and propane sorption in 6FDA-DABA.....	47
Figure 6.10 : CO ₂ /CH ₄ sorption in 6FDA-DABA.	48
Figure 6.11 : C ₃ H ₆ / C ₃ H ₈ sorption in 6FDA-DABA.....	48
Figure 6.12 : Accessible free volume distribution of 6FDA-DABA and 6FDA-DABA/sorbate systems.....	49
Figure 6.13 : Accessible free volume distribution of BTDA-DABA and BTDA-DABA/sorbate systems.....	49
Figure 6.14 : Accessible free volume distribution of 6FDA/BTDA-DABA and 6FDA/BTDA-DABA/sorbate systems.	50
Figure 6.15 : Accessible free volume distribution of polyimides/CO ₂ and copolyimide/CO ₂ systems.....	50
Figure 6.16 : Accessible free volume distribution of polyimides/C ₃ H ₆ and copolyimide/C ₃ H ₆ systems.	51
Figure 6.17 : Accessible free volume distribution of polyimides/C ₃ H ₈ and copolyimide/C ₃ H ₈ systems.	51
Figure 6.18 : Repeat unit of 6FDA-DABA.....	52
Figure 6.19 : Radial distribution functions of CO ₂ around F, N1, O1, O2 and O3 atoms of 6FDA-DABA.....	53

Figure 6.20 : Radial distribution functions of CO ₂ around F, N1, O1, O2 and O3 in 6FDA-DABA/CO ₂ system at a loading of 54 and 128 CO ₂	54
Figure 6.21 : Repeat unit of BTDA-DABA	55
Figure 6.22 : Radial distribution functions of CO ₂ around N1, O1, O2, O3 and O4 atoms of BTDA-DABA.....	55
Figure 6.23 : Radial distribution functions of CO ₂ around N1, O1, O2, O3 and O4 in BTDA-DABA/CO ₂ system at a loading of 83 and 198 CO ₂	56
Figure 6.24 : Repeat unit of 6FDA/BTDA-DABA	57
Figure 6.25 : Radial distribution functions of CO ₂ around F, N1, N2, O1, O2, O3, O4 and O5 atoms of 6FDA/BTDA-DABA at a loading of 61 CO ₂	57
Figure 6.26 : Radial distribution functions of CO ₂ around F, N1, N2, O1, O2, O3, O4 and O5 atoms of 6FDA/BTDA-DABA at a loading of 132 CO ₂	58
Figure 6.27 : Radial distribution functions of CO ₂ around F, N1, N2, O1, O2, O3, O4 and O5 in 6FDA/BTDA-DABA/CO ₂ system at a loading of 61 and 132 CO ₂	59
Figure 6.28 : FTIR spectrum of poly(amic acid) and polyimide of BTDA-DABA.....	60
Figure 6.29 : DSC thermogram of BTDA-DABA	62
Figure 6.30 : TGA thermogram of BTDA-DABA.....	63
Figure 6.31 : X-ray diffraction curve of synthesized BTDA-DABA.....	64
Figure A.1 : CO ₂ , propylene and propane sorption in BTDA-DABA.....	73
Figure A.2 : CO ₂ /CH ₄ sorption in BTDA-DABA.....	73
Figure A.3 : C ₃ H ₆ / C ₃ H ₈ sorption in BTDA-DABA.....	74
Figure A.4 : CO ₂ , propylene and propane sorption in 6FDA/BTDA-DABA	74
Figure A.5 : CO ₂ /CH ₄ sorption in 6FDA/BTDA-DABA.....	75
Figure A.6 : C ₃ H ₆ / C ₃ H ₈ sorption in 6FDA/BTDA-DABA.....	75

GAS SORPTION IN 3,5-DIAMINOBENZOIC ACID (DABA) BASED POLYIMIDES

ABSTRACT

Polyimides especially aromatic ones are promising materials for gas separation applications due to their outstanding thermal and separation properties which depend on chemical structure. Molecular simulation techniques can be used to obtain theoretical understanding of the relationship between chemical structure and the transport behavior of polyimide membranes. The objective of this study is to predict structure-property and structure-solubility relationships of polyimides at the atomistic level. In accordance with this purpose, structural properties and sorption behaviors of a copolyimide and its polyimides were estimated by using molecular simulation techniques. The polyimides and the copolyimide are comprised of 4,4-hexafluoroisopropylidene-diphthalic anhydride (6FDA) and 3,3',4,4'-benzophenone tetracarboxylic dianhydride (BTDA) as dianhydrides and 3,5-diaminobenzoic acid (DABA) as diamine.

The simulations were carried out using the *Accelrys Materials Studio* software, with all molecular interactions being modeled using the COMPASS force field. The simulation cells of 6FDA-DABA, BTDA-DABA and 6FDA/BTDA-DABA polyimides were constructed and structural properties were estimated with the help of the analysis tools available in the software. Grand Canonical Monte Carlo simulations were applied to estimate the sorption of CO₂, CH₄, O₂, N₂, propane and propylene molecules at different temperatures and pressures.

Comparison of estimated structural properties with available experimental data in the literature revealed a disagreement for BTDA-DABA. Based on the disagreement, the synthesis and characterization of BTDA-DABA were carried out. The polyimide is characterized by thermal gravimetric analysis (TGA), differential scanning calorimetry (DSC), and wide angle x-ray diffraction WA-XRD analyses.

Results obtained from experimental study of BTDA-DABA are close to our estimations and also the structural properties of 6FDA-DABA are in good agreement with the data available in the literature. Although polyimides and copolyimide show close structural properties fractional free volume, cohesive energy density, radius of gyration of BTDA-DABA are higher. The glass transition temperature of BTDA-DABA is higher than that value of 6FDA-DABA. The carbonyl bridge of BTDA is considered to be more rigid than hexafluoroisopropylidene bridge of 6FDA. Interchain spacings of 6FDA based polyimide and copolyimide are higher because of bulky bridging group. Except glass transition temperature, structural properties of 6FDA/BTDA-DABA is between its corresponding polyimides. Solubility of N₂, O₂, CO₂ and CH₄ in BTDA-DABA matrix and solubility of C₃H₆ and C₃H₈ in copolyimide matrix is higher. Ideal solubility selectivities of 6FDA-DABA in O₂/N₂, CO₂/CH₄ and C₃H₆/C₃H₈ systems are higher than others. The swelling of 6FDA/BTDA-DABA is stronger than its corresponding polyimides after CO₂, C₃H₆

and C₃H₈ sorption. Probing test method to obtain the accessible free volume distribution of polyimide and copolyimide matrices shows that an increase of the radius of the probing results in a decrease of the accessible free volume. Radial distribution function analyses revealed that CO₂ sorption in 6FDA-DABA occurs initially at the imide groups and hydroxyl oxygen site of DABA group, then at higher loadings of CO₂, interactions occurred strongly in oxygen of carboxyl and hydroxyl of DABA. CO₂ sorption in BTDA-DABA occurs initially at carboxyl of benzophenone and imide groups, at high loading preferential sites shifted to oxygen of hydroxyl group of DABA moiety. CO₂ sorption in 6FDA/BTDA-DABA occurs initially at the oxygen atoms at carboxyl of benzophenone and imide group of BTDA and in the case of high CO₂ loading strong interactions occurs at nitrogen of imide group of BTDA and oxygen of hydroxyl group of DABA.

3,5-DİAMİNOBENZOİK ASİT (DABA) BAZLI POLİİMİDLERDE GAZ SORPSİYONU

ÖZET

Aromatik poliimidler ısı, mekanik ve ayırma özelliklerinden dolayı umut vaadeden gaz ayırma malzemeleridir ve bu özellikleri kimyasal yapılarına bağlıdır. Moleküler simülasyon teknikleri, poliimid membranların ayırma özellikleriyle kimyasal yapıları arasındaki ilişkiyi daha iyi anlamada kullanılabilir. Bu çalışmanın amacı poliimidlerde yapı/performans ilişkisinin atomik düzeyde incelenmesidir. Bu amaç doğrultusunda moleküler simülasyon tekniklerini kullanarak 4,4-hekzafloroizopropiliden-diftalik anhidrid (6FDA), 3,3',4,4'-benzofenon tetrakarboxilik dianhidrid (BTDA) ve 3,5-diaminobenzoik asit (DABA) den türetilen 6FDA-DABA, BTDA-DABA poliimidleri ile 6FDA/BTDA-DABA kopoliimidinin yapısal özellikleri ve sorpsiyon davranımları incelenmiştir.

Simülasyonlar *Accelrys Materials Studio* simülasyon paketi kullanılarak gerçekleştirilmiş ve moleküler etkileşimler bu paketin içerisinde mevcut olan COMPASS kuvvet alanı kullanılarak modellenmiştir. Poliimidlerin ve kopoliimidin yapısal özellikleri simülasyon paketinin içinde mevcut olan analiz araçları ile hesaplanmıştır. CO₂, CH₄, O₂, N₂, propan ve propilen gazlarının farklı sıcaklık ve basınçlarda çözünürlük katsayıları Büyük Kanonik Monte Karlo simülasyonları ile hesaplanmıştır.

Simülasyon çalışmalarıyla elde edilen verilerin BTDA-DABA için literatürde var olan deneysel çalışmayla uyum göstermediği görülmüştür ve bu poliimidinin sentezi ve karakterizasyonu gerçekleştirilmiştir. Sentezlenen poliimid Termogravimetrik Analiz (TGA), Diferansiyel Taramalı Kalorimetre (DSC) ve Geniş Açılı X-ışını Saçılması (WA-XRD) yöntemleri ile karakterize edilmiştir.

BTDA-DABA için deneysel çalışmayla elde edilen sonuçlar simülasyon çalışmasıyla tahmin edilen değerlere yakın sonuçlar vermektedir. 6FDA-DABA için tahmin edilen yapısal özellikler ise literatürdeki verilerle uyum içersindedir. Kopoliimid ve poliimidler yapısal olarak benzer özellikler gösterebilir, BTDA-DABA poliimidinin serbest hacim fraksiyonu, kohesive enerji yoğunluğu ve dönüş yarıçapı daha yüksektir. BTDA-DABA'nın camı geçiş sıcaklığı 6FDA-DABA'ninkinden daha yüksektir. BTDA monomerinin karbonil köprü grubunun 6FDA monomerinin hekzafloroizopropiliden köprü grubundan daha rijit olduğu kabul edilebilir. Camı geçiş sıcaklığı dışında 6FDA/BTDA-DABA kopoliimidinin yapısal özellikleri poliimidlerinin arasında değer vermektedir. N₂, O₂, CO₂ ve CH₄ gazlarının BTDA-DABA poliimidinde, C₃H₆ ve C₃H₈ gazlarının ise 6FDA/BTDA-DABA kopoliimidinde çözünürlükleri daha yüksektir. O₂/N₂, CO₂/CH₄ ve C₃H₆/C₃H₈ gaz karışımları için 6FDA-DABA poliimidinin ideal çözünürlük seçicilikleri daha yüksektir. Kopoliimidin ve poliimidlerin erişilebilir serbest hacim dağılımını elde etmek için probing test yöntemi uygulanmış ve gazların kinetik yarıçaplarına denk düşen prob değerlerinde erişilebilir serbest hacmin azaldığı görülmüştür. Radyal dağılım fonksiyonu sonuçlarına göre, CO₂ gazının 6FDA-DABA poliimidinde

sorpsiyonu öncelikle imid grubu ve DABA monomerinin hidroksilindeki oksijen atomunda gerçekleşmektedir. Daha yüksek CO₂ yüklemelerinde ise gaz ile poliimidin etkileşimi DABA grubunun karbonil ve hidroksilindeki oksijen atomlarında gerçekleşmektedir. CO₂ gazının BTDA-DABA poliimidinde sorpsiyonu öncelikle imid grubu ve BTDA monomerinin karbonil köprüsündeki oksijen atomunda gerçekleşmektedir. Daha yüksek CO₂ yüklemelerinde ise gaz ile poliimidin etkileşimi DABA grubunun hidroksilindeki oksijen atomlarında gerçekleşmektedir. CO₂ gazının 6FDA/BTDA-DABA kopoliimidindeki sorpsiyonu ise öncelikle BTDA-DABA yapısının imid grubu ile BTDA monomerinin karbonil köprüsündeki oksijen atomunda gerçekleşmektedir. Daha yüksek CO₂ yüklemelerinde ise imid gruplarındaki azot atomu ile DABA grubunun hidroksilindeki oksijen atomlarında daha güçlü etkileşim gözlenmiştir.

1. INTRODUCTION

Membrane based gas separation processes become a significant separation technology for commercially available gas mixtures. The separation of a gas mixture is based on the transport of one or more components from one side of a selectively permeable surface to another side by a driving force. Gas separation through membranes is best described by the solution-diffusion model that estimates the transport of gases into three step [1]; 1) Sorption of gas into the membrane, 2) Diffusion through the membrane due to an applied concentration gradient, and 3) Desorption of the gas.

Membrane based processes are attractive because of following reasons: process needs low initial investment cost and consumes low energy, the capacity expansion and integration with other separation processes can be done easily, and separation is carried out continuously.

In commercial applications, a membrane is desired to be both highly permeable and highly selective. In addition, commercially attractive membranes should be thermally, chemically and mechanically stable. While high selectivity provides high product purity and ensures more efficient separation process, high permeability decreases investment and operating costs of membrane system by reducing the required membrane area and driving force.

Polyimides, especially aromatic ones, attract attention in membrane based gas separation applications compared to many other polymeric materials due to their high thermal stability, chemical resistance and good mechanical characteristics. Preparation of polyimide membranes with highly permeable and highly selective is an essential in separation applications of commercially important gas pairs such as O_2/N_2 , CO_2/CH_4 , H_2/CH_4 , H_2/N_2 and olefin-paraffin. However, a trade-off exists between permeability and selectivity that is known as polymer upper bound limit. A permeability-selectivity trade-off curve for gas pairs such as O_2/N_2 , CO_2/CH_4 ,

H_2/CH_4 and for others were described by Robeson in 1991[2] and 2008[3], which is shown for H_2/N_2 pairs in Figure 1.1.

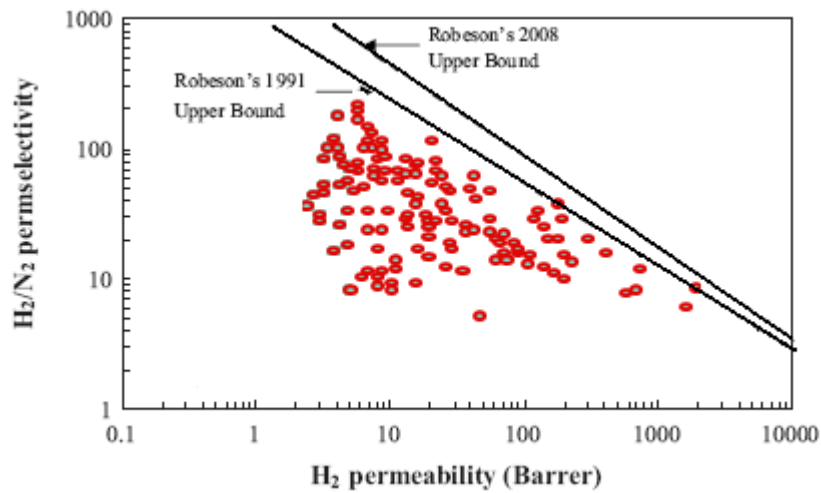


Figure 1.1: Robeson curve for H_2/N_2 separation application.

The upper bound of the curve represents commercially attractive region. Therefore, production of membrane materials in upper limit has great importance for using membrane technology in gas separation processes.

Although, experimental studies about polyimides have been increased in recent years, high permselectivity for commercial applications could not be obtained. For that reason, molecular simulation can be an important tool for developing attractive membrane materials by predicting structure-solubility relationships of polyimides at the atomistic level prior to experimental studies.

The main purpose of this thesis is to obtain effective and commercially attractive polyimide membranes for gas separation applications. Therefore, it is aimed to predict sorption behaviour of light gases and gas pairs as well as hydrocarbons on 6FDA/BTDA-DABA copolyimide, which is studied by Halitoğlu et.al [4] by using group contribution method and proposed one of promising copolyimide structure. Also structure-property and structure-solubility relationships of this copolyimide and its polyimides, 6FDA-DABA and BTDA-DABA, are investigated via molecular simulation. Moreover the synthesis and the characterization of BTDA-DABA were carried out and the results were compared with the results that were obtained by simulation study.

2. THEORY AND BACKGROUND

This section includes brief information about theoretical background of gas transport mechanisms through membrane and a literature review of previous studies on structure-property and structure-solubility relationships of polyimide membranes.

2.1 Gas Transport Mechanism Through Membranes

Membrane based gas separation processes have proved their outstanding properties for the separation of commercially important gas pairs such as O_2/N_2 , CO_2/CH_4 , H_2/CH_4 , H_2/N_2 and olefin-paraffin. In the simplest sense, a membrane is used to separate mixtures of gases in a feed stream, and generate a permeate rich in a specific gas. Gas separation membranes are selective which means one component of mixture passes through while the others are being rejected. Permeate stream sorbs the gas into the membrane and the gas diffuse down a sorbed concentration gradient, and are collected on the downstream side of the membrane. The non-permeating species is purged via the unfiltered stream [5]. The driving force for permeation is chemical potential difference across the thickness of the material. A schematic representation of gas separation through a membrane is shown in Figure 2.1.

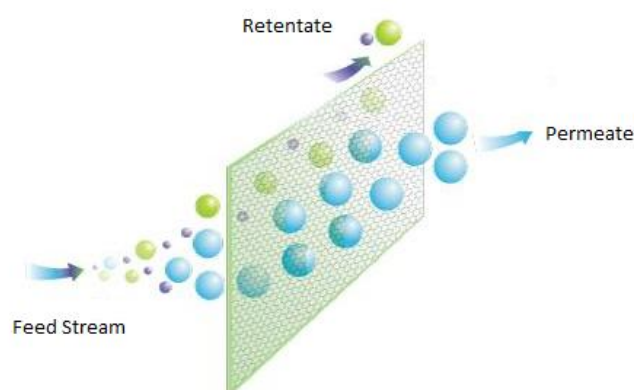


Figure 2.1: Schematic representation of gas separation through a membrane [6].

In literature various mechanisms are presented to describe transport behavior through non-porous membranes. While thermodynamic and mechanical principles are used to explain models, some are based upon the correlations between the observed transport

behavior and the physical characteristics of membrane material. The most important models [7] are Knudsen diffusion, surface diffusion, capillary condensation, molecular sieving and solution-diffusion mechanism.

In Knudsen diffusion, gas molecules moves through pores which are small enough to prevent bulk diffusion. The migration of gas molecules along the pore walls of a porous membrane is modeled with surface diffusion. The rate, which indicates the efficiency of separation, is determined by the intensity of interaction between the pore walls and the adsorbed gas. Capillary condensation occurs when sorbed gas molecules partially condensate thus condensed gas molecules diffuse faster through pores and separation is achieved. In molecular sieving, gas molecules are separated by size exclusion.

Gas separation through membranes is best described by the solution diffusion model. This model describes the transport of gases as a three step process [8]:

1. Sorption of the penetrant in the membrane,
2. Diffusion of the penetrant through the membrane due to an applied concentration gradient,
3. Desorption at the opposite interface.

At the feed side, molecules of a given component dissolve in the membrane phase and thermodynamic equilibrium exists between the penetrants sorbed in the membrane phase and the penetrants in the feed or permeate side compartment. The chemical potential of this component at the downstream side is lower than that at the feed side which means that its concentration at the membrane downstream side is also lower. This driving force causes a continuous diffusional mass transport of the component through the membrane.

Both the sorption/desorption and diffusion steps are dependent on the physical properties of the membrane material and the penetrant. Sorption models are based on the thermodynamics of the penetrant-membrane interaction, whereas the diffusion is primarily modeled with Fick's laws of diffusion [9].

2.2 Polyimide Membranes for Gas Separation Applications

Gas transport through glassy polyimides has been studied because of their outstanding separation properties [5]. In order to describe the observed transport behavior, different models were proposed based upon molecular-kinetic, phenomenological, and thermodynamic considerations [10]. These models are based on three different theories [10]: the “hole” vacancy theory, the activated complex theory and the fluctuation theory.

In the hole vacancy theory, it is assumed that polymer matrix creates or expands a hole for the gas molecule which diffused through this successful creations and expansions. The activated complex theory defines the movement of gas molecules through the matrix with an efficient energy to conquer a potential energy barrier. The fluctuation theory based on density or volume fluctuations in the matrix occurred by thermal activations. These fluctuations lead an excess space in which gas molecules pass through.

2.2.1 Free volume in polyimides

All three explanations mentioned above are derived from the free volume theory. This theory claims that the movement of gas molecules in polymer matrix is not only dependent on the available free volume but also on the sufficient energy of gas molecules to beat effective forces between chains. The presence of free volume within the polymer, which was first proposed by Fujita in 1960 [10], is related to limitations in mobility that induces the non-equilibrium state of the polymer. The concept is based on the presence of different types of free volume in polyimides: the interstitial free volume and the hole free volume. For example, backbone rotations of some polymers are not thermally allowed which leads a rigid helical structure for the polyimide thus free volume is formed by the interstitial space between neighboring helices, and gas transport occurs through this channel-like free volume. On the other hand, some polymers exhibit a flexible backbone, which leads to the formation of irregular voids (holes). In this case, gas molecules are free to move within the voids. The presence of free volume of polymers are expressed by the fractional free volume (FFV) model which provides an estimation for gas transport in polymeric membranes roughly but fails especially for the transport of highly condensable gases [11].

2.2.2 Gas transport in glassy polyimides

The gas transport behavior of dense polymeric membranes is widely investigated by employing the solution-diffusion model [12]. The model assumes that a polymer comprises continuous chain matrix with micro voids (holes). These micro voids are caused by the non-equilibrium thermodynamic state of glassy polymers. Based on this model, the gas permeability (P) across the membrane is the product of solubility (S) and diffusivity (D).

$$P = S \times D \quad (2.1)$$

The permselectivity ($\alpha_{A,B}$) of the ideal gas pair A and B covers the solubility (S_A/S_B) and diffusivity (D_A/D_B) selectivities.

$$\alpha_{AB} = \frac{P_A}{P_B} = \left(\frac{S_A}{S_B} \right) \times \left(\frac{D_A}{D_B} \right) \quad (2.2)$$

Different models have been studied to describe the sorption and diffusion of penetrant molecules in glassy polymers but most widely used model is the dual-mode sorption theory which is defined in terms of Henry's law of solubility (dissolution in continuous chain matrix) and Langmuir-type of sorption (sorption in microvoids). The basic assumptions of this model are [12]:

1. The two modes occur simultaneously and are always in equilibrium.
2. The penetrants sorbed under Langmuir mode are completely immobilized.
3. Diffusion occurs only in the dissolved mode and the diffusion coefficient is independent of concentration.

In dual-mode sorption theory, the gas concentration in the polymer for an applied pressure (p) is expressed as:

$$C = C_D + C_H = k_D p + \frac{C'_H b p}{1 + b p} \quad (2.3)$$

where

C : the total penetrant concentration

C_D : concentration by Langmuir sites.

C_H : concentration by Henry sites.

k_D : Henry's solubility constant.

C'_H : Langmuir hole saturation constant

b : Langmuir affinity constant which represents the ratio of the rate constants of gas adsorption and desorption in the microcavities or defects.

p : pressure.

The solubility coefficient (S) (Eqn.2.4) is the ratio of total penetrant concentration to pressure.

$$S = \frac{C}{p} = k_D + \frac{C'_H b}{1 + bp} \quad (2.4)$$

The schematic representation of Henry sorption, Langmuir sorption, and dual-mode sorption is shown in Fig.2.2.

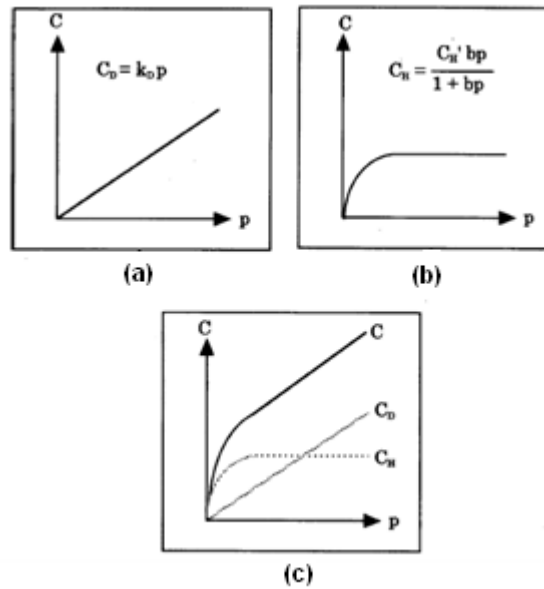


Figure 2.2: Schematic representation of Henry sorption (a), Langmuir sorption (b) and dual-mode sorption (c) [13].

In dual mode, sorption into unrelaxed free volume of the polyimide can be described by the Langmuir model however at high pressures this free volume becomes saturated, and then the Henry's law is used [13].

According to assumptions of the model the diffusion coefficient is independent of concentration thus Arrhenius equation is used to express diffusion coefficient (D).

$$D = D_o \exp\left(\frac{-E_D}{RT}\right) \quad (2.5)$$

where, D_0 is the pre-exponential factor, R is the gas constant, T is the temperature (K) and E_D is the activation energy for diffusion.

The explanation of difference in inherent gas diffusion of the Langmuir and Henry sites in dual mobility model was proposed by Paul and Koros [14-15]. This model is presented in equation 2.6.

$$P = k_D \left(1 + \frac{FK}{1 + bp_2} \right) D_D \quad (2.6)$$

where; F is the ratio of D_H to D_D , D_D and D_H are the diffusion coefficients in the Henry and Langmuir sites, respectively, p_2 is the pressure at the upstream boundary and K is defined as:

$$K = \left(\frac{C'_H b}{k_D} \right) \quad (2.7)$$

2.2.3 Plasticization in polyimides

In glassy polymers, an increase in segmental motion of polymer chain is called plasticization. This increased mobility augments the frequency of free volume and the average size of holes. Sanders [16] suggested that the movement of side groups on polymer chains may decrease the local packing that let the small penetrant molecules pass through membrane.

In the presence of a gas pair, swelling in the matrix causes an increase in the fractional free volume of the polymer and thus the permeability of both components increases but the selectivity decreases [17]. For example, CO_2 plasticize the CO_2/CH_4 membrane separation system at elevated pressures [18]. Due to the presence of CO_2 , the polymer matrix swells during the sorption. This plasticizing effect accelerates the CH_4 permeation thus the membrane system loses its selectivity. Both sorption and diffusion coefficients may deviate from the simple dual mode expressions due to the increase in segmental motion after the swelling of the polymer [17]. Various models have been proposed to describe plasticization behavior. Stern and Saxena [19] modified the dual mode transport model to describe the transport of gases in and through glassy polymer membranes which are plasticized by the penetrants. Mauze and Stern [20] modified this model by neglecting the concentration associated with

Langmuir sorption mechanism and Zhou and Stern [21] studied the impacts of plasticization on the penetrant transport in the Henry's law and Langmuir domains separately.

2.3 Review of Structure-Solubility Relationship in Polyimides

Aromatic polymers such as polysulfones, polycarbonates and polyimides have considerable potential as membrane material for gas separation. However, polyimides are thermally stable and high performance polymers which provide them required specifications for being employed in high temperature and high performance gas separation. In addition, they can be packed in the form of modules with high surface area and they can be used as thin, defect-free, low-cost membranes. The synthesis of polyimide proceeds according to polycondensation reaction of equimolar amount of diamine and dianhydride in an aprotic solvent to form polyamic acid. The dehydration of poly(amic acid) results in chemically stable polyimide formation.

Wang et al. [22] studied synthesis and characterization of aromatic polyimides formed by BTDA and 6FDA dianhydrides with various sizes of alkyl sidechain. They reported that the glass transition temperature of BTDA based polyimides exceeded that of the 6FDA based ones. They found that thermal stability of sidegroup containing polyimides are low than the unsubstituted polyimides.

Park et al. [23] studied on gas separation properties of 6FDA based polyimides having a hydroxyl or carboxyl polar group. They found that polar group-containing polyimides showed low CO₂ permeability except that they showed high separation selectivity for CO₂/N₂ and CO₂/CH₄. 6FDA polyimide membranes with phenylenediamine having over 3 methyl group exhibited relatively low selectivity but high permeability of CO₂. They also reported that gas permeabilities and diffusion coefficients for the polar group-containing polyimide membranes showed similarity.

Shimazu et al. [24] studied the effect of the chemical structures on the physical and gas permeation properties of the 40 different 6FDA based polyimides. They investigated permeability of propane and propylene at 298 K. They found that polyimides that have high glass transition temperatures and large fractional free

volumes showed high permeability and low permselectivity for propylene/propane mixed-gas system. The –CONH– bridge between the phenylene linkage restricts the solubility of propylene, however the –Cl substituent in the phenylene linkage exhibits high separation properties for propylene/propane mixture.

Zhang et al. [25] examined the CO₂-induced plasticization of polyimide derived from 6FDA and 4,4'-oxydianiline (ODA) both experimentally and in atomistic level. The radial distribution functions between CO₂ and typical atoms of polyimide showed that the imide group is the favourable site. With increasing CO₂ loading, they found that the polyimide membrane exhibits a depressed glass transition temperature, a dilated volume, an increased fractional free volume. They suggested that the plasticization could be controlled by fewer substitution of the ether groups which have a stronger effect on the mobility of polyimide chains at high pressures.

Kang et al. [26] used an atomistic modelling technique to develop some structure-property relationships of four BTDA based polyimides. They used Dreiding force field [27] to model interactions and Monte Carlo method to assign dihedral angles along the chain backbone of each polyimide. They used Molecular Dynamics method to optimize final structure and Molecular Mechanics to obtain mechanical properties of polyimides. They found that polyimide with an oxygen linkage has the most flexible backbone and polyimide with a sulfonyl linkage had the most rigid one. A more flexible chain backbone results higher degree of conformational state, small characteristic ratio, low solubility parameter, low elastic modulus and large yield strain.

Pan et al. [28] applied a molecular simulation technique in order to develop structure and property relationships of three polyimides with different lengths of methylene spacing groups in biphenyl side chain of the diamines moiety. They modeled the interaction by using Dreiding 2.21 force field [29]. They found that polyimide with six methylene spacing groups has conformational structure which decreases the energy barrier in rotational bonds of the backbone resulting a decrement in glass transition temperatures.

3. MOLECULAR SIMULATION METHODS

Molecular simulation is a computational method that is used to predict physical and chemical properties of systems prior to experimental studies. Molecular based simulations are widely applied to many systems. Calculation of intermolecular energies or forces and predictions of the thermodynamic, mechanical, permeability, electrical, optical and other properties of theoretical model is accurately done in atomistic level.

In this section, the basic concepts of the statistical ensembles, molecular forcefields, molecular dynamics and Monte Carlo methods will be briefly summarized.

3.1 Statistical Ensembles

An ensemble is a collection of systems described by the same set of microscopic states with common set of macroscopic attributes [30]. An ensemble consists of a large number of theoretical copies of a system that represents a possible state that the real system might be in. The complexity of real systems makes the characterization of system difficult via molecular simulation. Therefore, to characterize and calculate overall properties of the whole system statistical ensembles should be established at first. According to external macroscopic parameters the state of a system are denoted by statistical ensembles. These macroscopic parameters must be same with the corresponding real systems.

Table 3.1 presents common statistical ensembles with their partition function and related thermodynamic property. The partition function (Z) is the sum of all different probabilities of the system and encodes the statistical properties in thermodynamic equilibrium. As seen from Table 3.1 thermodynamic functions are expressed with the characteristic partition function of each ensemble. Helmholtz free energy is expressed by partition function of canonical ensemble. While pressure is obtained by grand canonical ensemble, entropy and Gibbs free energy are estimated from microcanonical and isothermal-isobaric ensembles, respectively.

Table 3.1: Statistical Ensembles [31]

Statistical ensemble	Imposed variables	Partition function (Z)	Thermodynamic potential
Canonical	N, V, T	$\sum_i e^{-\beta E_i(N,V)}$	$A = -kT \ln Z_{NVT}$
Grand Canonical	V, T, μ	$\sum_i e^{\beta N\mu} Z_{NVT}$	$PV = -kT \ln Z_{\mu VT}$
Microcanonical	N, V, E	$\sum_i \delta(E_i - E)$	$S = k \ln Z_{NVE}$
Isothermal-Isobaric	N, P, T	$\sum_i e^{\beta p V_i} Z_{NVT}$	$G = -kT \ln z_{NPT}$

Grand canonical ensemble (μVT) implies open systems in which the particle number is changeable. This statistical ensemble is favourably suitable for treating physical system in which particles and energies can be transported crosswise the system boundaries [32]. For example sorption behavior of materials is characterized by using grand canonical ensemble.

Canonical (NVT), microcanonical (NVE) and isothermal-isobaric (NPT) ensembles denote closed systems that the number of particles is fixed. Information about temperature and pressure of a system is more available than information about energy; therefore, usage of microcanonical ensemble is rare in molecular simulation. Nonetheless, this ensemble is favored to calculate the transport properties.

In many physical processes, the number of molecules is remained constant and the process is carried out at fixed pressure and temperature so canonical and isothermal-isobaric ensembles will be a more suitable representation of the real system.

3.2 Molecular Forcefields

A forcefield is a molecular model that represents the potential energy of the model by describing interactions of atoms and molecules in the system. Reliability of molecular simulation calculation depends on the forcefield. Therefore, the most critical step of molecular simulation is to select an appropriate forcefield in accordance with properties of interest [33]. This is important because the selected forcefield should represent the structural and dynamical properties of a system accurately in thermodynamical equilibrium.

The total energy (E_{total}) of a system is the sum of two interaction terms: interactions between bonded atoms, and non-bonded atoms.

$$E_{total} = E_{bonded} + E_{non-bonded} \quad (3.1)$$

Bonded and non-bonded terms of intermolecular and intramolecular interactions are summarized in Figure 3.1[33-34].

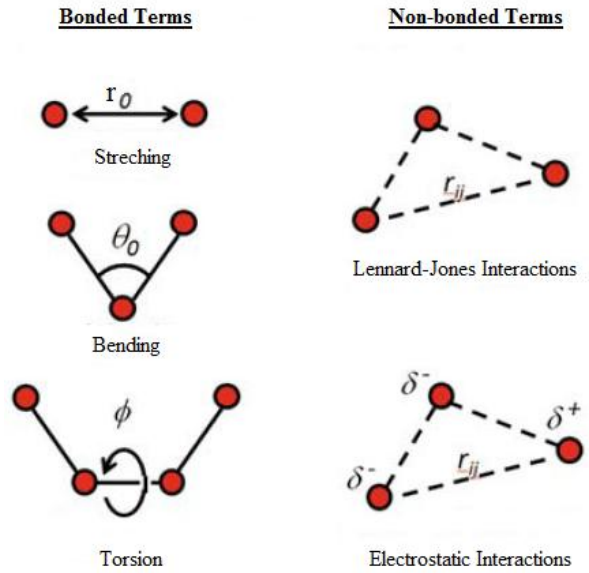


Figure 3.1: Intermolecular and intramolecular interactions.

The bonded potential includes three main contributors; energy of bond stretching, energy of angle bending and energy of angle torsion.

$E_{stretching}$ is energy of bond strain between two atoms and is used to calculate deformation energy that is originated by shrinking of bonds. This term is expressed as Equation 3.2.

$$E_{stretching} = \frac{1}{2}k_b(r - r_0)^2 \quad (3.2)$$

where r is the length of bond, r_0 is the ideal bond length and k_b is stretching constant[35].

$E_{bending}$ is deformation energy of bonds between three atoms. It is generated by the diversity of angles of these atoms. It is stated as Equation 3.3.

$$E_{bending} = \frac{1}{2}k_\theta(\theta - \theta_0)^2 \quad (3.3)$$

where θ is the angle between bonds, θ_0 is ideal value of angle and k_θ represents bending constant.

$E_{torsion}$ is energy that takes its source from the change of angle of a plane that is composed four atoms. It needs a periodic function to be calculated. Torsional energy is represented as:

$$E_{torsion} = \frac{1}{2} k_{\phi} (1 + \cos(n\phi - \phi_0)) \quad (3.4)$$

where ϕ is the torsional angle between planes, n is periodic number, ϕ_0 is ideal torsional angle and k_{ϕ} is torsional constant.

Beside energy of stretching, energy of bending and energy of torsion, the bonded potential includes cross terms which are the combination of two or three internal coordinates (bond-bond, bond-angle, angle-angle, angle-torsion, and bond-torsion-angle).

Independent molecules and atoms interact through non-bonded forces. The non-bonded interactions are through-space interactions and are usually modelled as a function of some inverse power of distance. The non-bonded potential consists of two terms, the electrostatic interactions and the dispersive interactions between molecules:

$$E_{non-bonded} = E_{dispersive} + E_{electrostatic} \quad (3.5)$$

In this study, dispersive interactions are modelled with a Lennard-Jones pair potential and are carried out for all particle pairs. Lennard-Jones potential is represented as:

$$E^{LJ} = \sum_{\substack{i,j \\ i < j}} 4\epsilon_{ij} \left(\left(\frac{\sigma_{ij}}{r_{ij}} \right)^{12} - \left(\frac{\sigma_{ij}}{r_{ij}} \right)^6 \right) \quad (3.6)$$

where r_{ij} is the distance between the interacting particles i and j , ϵ is the energy parameter, and σ_{ij} is the finite distance at which the inter-particle potential is zero.

The electrostatic term is calculated from the Coulombic interaction between point charges. Coulombic interaction is defined in Eqn.3.7 where ϵ_o is the electric constant and q_i, q_j the charges of particles i and j [33-34].

$$E_{Coulomb} = \sum_{\substack{i,j \\ i < j}} \frac{1}{4\pi\epsilon_o} \frac{q_i q_j}{r_{ij}} \quad (3.7)$$

Many different forcefields exist, such as AMBER [36], widely used for modeling proteins and DNA, or CHARMM (Chemistry at HARvard Macromolecular Mechanics) [36-37], PCFF (Polymer-Consistent Force Field) [38-39] and CVFF (Consistent Valence Force Field) [39], used for macromolecules and proteins, DREIDING [27], GROMOS [37] ve GROMACS (GRONingen Machine for Chemical Simulations) and COMPASS (Condensed-phase Optimized Molecular Potentials for Atomistic Simulation Studies) [40].

COMPASS is the first ab initio forcefield that enables an accurate and simultaneous prediction of various gas-phase and condensed-phase properties of organic and inorganic materials. It is specially designed for modelling of complex molecules' interactions. Consequently, structural, conformational, vibrational, and thermophysical properties and lattice energies of various isolated and condensed molecules can be precisely predicted by using COMPASS forcefield . All terms that constitute this forcefield is represented in Eqn.3.8.

$$\begin{aligned}
E_{Total} &= E_b + E_\theta + E_\phi + E_\chi + E_{bb'} + E_{b\theta} + E_{b\phi} + E_{\theta\theta'} + E_{\theta\phi} + E_{\theta\phi'} + E_{Coulomb} + E_{LJ} \\
&= \sum_b \left[K_2 (b - b_0)^2 + K_3 (b - b_0)^3 + K_4 (b - b_0)^4 \right] + \\
&\sum_\theta \left[H_2 (\theta - \theta_0)^2 + H_3 (\theta - \theta_0)^3 + H_4 (\theta - \theta_0)^4 \right] + \\
&\sum_\phi \left[V_1 (1 - \text{Cos}\phi) + V_2 (1 - \text{Cos}2\phi) + V_3 (1 - \text{Cos}3\phi) \right] + \sum_\chi K_\chi (\chi - \chi_0)^2 + \\
&\sum_{b,b'} F_{b,b'} (b - b_0) (b' - b_0') + \sum_{b,\theta} F_{b,\theta} (b - b_0) (\theta - \theta_0) + \\
&\sum_{b,\phi} (b - b_0) \left[F_{b,\phi}^{(1)} (\text{Cos}\phi) + F_{b,\phi}^{(2)} (\text{Cos}2\phi) + F_{b,\phi}^{(3)} (\text{Cos}3\phi) \right] + \\
&\sum_{\theta,\theta'} F_{\theta,\theta'} (\theta - \theta_0) (\theta' - \theta_0') + \sum_{\theta,\phi} (\theta - \theta_0) \left[F_{\theta,\phi}^{(1)} (\text{Cos}\phi) + F_{\theta,\phi}^{(2)} (\text{Cos}2\phi) + F_{\theta,\phi}^{(3)} (\text{Cos}3\phi) \right] + \\
&\sum_{\theta,\theta',\phi} F_{\theta,\theta',\phi} (\theta - \theta_0) (\theta' - \theta_0') \phi (\phi - \phi_0) + \sum_{i,j} \frac{q_i q_j}{r_{i,j}} + \sum_{i,j} \epsilon_{ij} \left[2 \left(\frac{r_{ij}^0}{r_{ij}} \right)^9 - 3 \left(\frac{r_{ij}^0}{r_{ij}} \right)^6 \right]
\end{aligned}$$

(3.8)

The Eqn. 3.8 can be divided into two categories: bonded terms, which include diagonal and off-diagonal cross terms, and nonbond interaction terms. The bonded terms represent internal coordinates of bond (b), angle (θ), torsion angle (φ), and outoff- plane angle (χ), and the cross terms include combinations of two or three

internal coordinates (bond-bond, bond-angle, angle-angle, angle-torsion and bond-torsion-angle). The nonbond interactions include a Coulombic function for an electrostatic interaction and a Lennard-Jones-9-6 function for the van der Waals term.

3.3 Molecular Dynamics Methods

Molecular dynamics (MD) is a deterministic method that integrates Newton's equations of motion for all particles in a system in order to obtain new configurations. This method allows the time-dependent properties of the system. The force on a moving particle is represented in Eqn.3.9, where m is the mass, a is the acceleration, and F is the force on the particle.

$$F_i = m_i a_i \quad (3.9)$$

Acceleration can be defined as:

$$a_i = \frac{F_i}{m_i} = \frac{d^2 r_i}{dt^2} \quad (3.10)$$

where, r represents the position of the particle and t is time. This equation is the basis of dynamic behavior. By integration of Eqn. 3.10 with respect to time (Eqn.3.11), applying the initial condition (Equation 3.12), ($v=v_i$ at $t=0$, where v is the velocity), and once again integrating with respect to time, Equation 3.13 is obtained,

$$\frac{dr_i}{dt} = \left(\frac{F_i}{m_i} \right) t + c_1 \quad (3.11)$$

$$c_1 = v_i \quad (3.12)$$

$$r_i = v_i t + \frac{a_i t^2}{2} + c_2 \quad (3.13)$$

where c_2 is the initial position of the particle. Using the last equation, it is possible to calculate the position of the particle only with its initial velocity and acceleration [41].

Different types of algorithms can be used to solve the equation of motion. Verlet algorithm and its modifications are the most frequently used ones. Verlet algorithm is based upon Taylor series expansion (Equation 3.14-16):

$$r(t + \Delta t) = r(t) + \frac{dr}{dt} \Delta t + \frac{1}{2!} \frac{d^2 r}{dt^2} \Delta t^2 + \dots \quad (3.14)$$

$$r(t - \Delta t) = r(t) - \frac{dr}{dt} \Delta t - \frac{1}{2!} \frac{d^2 r}{dt^2} \Delta t^2 - \dots \quad (3.15)$$

The combination of these equations gives the Verlet algorithm (Equation 3.16):

$$r(t + \Delta t) = 2r(t) - r(t - \Delta t) + \frac{d^2 r}{dt^2} \Delta t^2 \quad (3.16)$$

As an advantage, this algorithm allows determination of the molecular positions without velocity calculation. However, velocities are fundamental in kinetic energy calculation. So that the velocity can be obtained from Equation 3.17.

$$v(t) = \frac{r(t + \Delta t) - r(t - \Delta t)}{2\Delta t} \quad (3.17)$$

The Verlet is time reversible and has negligible energy drift for long times, this is essential in order to describe systems with constant energy. As a result the algorithm conserves energy for long time steps. Higher order algorithms let usage of larger time steps, but in general they have large long-time energy drift and this issue requires more calculation time [42].

The velocity term is one step behind the coordinates. In order to take this concern away, some modifications are applied to the algorithm. The modified algorithms are the Leap-frog Verlet Algorithm and the Velocity Verlet Algorithm. In Leap-frog Algorithm even velocity calculations are provided at half time intervals resulting in new position calculations, velocity and positions are still not defined simultaneously. Velocity Verlet Algorithm makes it possible to calculate both velocity and the position at the same time (Equation 3.18-20) [41-43].

$$r(t + \Delta t) = r(t) + v(t)\Delta t + \frac{a(t)\Delta t^2}{2} \quad (3.18)$$

$$v\left(t + \frac{\Delta t}{2}\right) = v(t) + \frac{a(t)\Delta t}{2} \quad (3.19)$$

$$v(t + \Delta t) = v\left(t + \frac{\Delta t}{2}\right) + \frac{a(t + \Delta t)\Delta t}{2} \quad (3.20)$$

For realistic representation of an ensemble the equation of motion has to be adjusted. This adjustment should comprise a thermostat and/or a barostat. Various methods have been developed to control system temperature and pressure. Simple velocity scaling, heat-bath coupling, Berendsen, Andersen, Nosé and Hoover are the basic methods that used for temperature control. Modified methods of Berendsen, Andersen, Hoover and Constraint are employed for pressure control.

In this study Berendsen method was used as both thermostat and barostat. With the Berendsen thermostat the system is connected with a heat bath and the deviation of system temperature is adjusted with a time constant τ that is added to the equation of motion [44].

$$\frac{dT}{dt} = \frac{T_0 - T}{\tau} \quad (3.21)$$

Next, all velocity are corrected by the factor:

$$\lambda = \left[1 + \frac{\Delta t}{\tau_T} \left\{ \frac{T_0}{T\left(t - \frac{\Delta t}{2}\right)} - 1 \right\} \right]^{1/2} \quad (3.22)$$

Similar to the temperature coupling, with Berendsen barostat pressure fluctuation is fixed with a time constant τ_p term.

$$\frac{dP}{dt} = \frac{P_0 - P}{\tau_p} \quad (3.23)$$

To correct cell size variations, cell volume is rescaled by a factor η . The coordinates are regulated by η^3 . This rescaling factor is:

$$\eta = 1 - \frac{\beta \Delta t}{\tau_p} (P_{ext} - P) \quad (3.24)$$

where β is isothermal compressibility.

The advantage of Berendsen control method is that it has little influence on kinetics and does not induce any oscillation in dynamic properties [45].

3.4 Monte Carlo Methods

The Monte Carlo (MC) method is a stochastic technique that is based on the use of random numbers and probability statistics. By applying MC methods, large and complex systems can be described in a number of random configurations. These configurations are generated by random changes of species position, both with suitable orientations and conformations[46].

In an MC simulation, the following steps are carried out respectively; a random trial configuration is generated initially, then for this trial configuration changes in energy and other properties are calculated, and an acceptance criterion is constituted, next the acceptance criterion is compared to a random number and the trial configuration is either accepted or rejected.

Sampling rule is one of fundamental term of MC method. Two types of sampling includes in MC method; simple sampling and importance sampling. In simple sampling technique, each point has equal probability. However not all point contributes to the solution equally, some have larger and some have smaller proportion therefore, sampling rule is an advantage where contribution to the solution is a lot. This type of sampling is called “importance sampling”. The difference sampling types is shown in the integral expressions in Equations 3.27-28.

Simple sampling,

$$I = \frac{1}{N} \sum_i^N f(x_i) \quad (3.26)$$

Importance sampling,

$$I = \sum_i^N \frac{f(x_i)}{p(x_i)} \quad (3.27)$$

In the equations above, p represents the probability and f represents the function that is integrated. It is obvious from equations that all points contribute the solution with the reverse of the probability in importance sampling.

In MC method, there are different types of MC moves: translation, rotation and volume change, etc. Translation is one of the MC moves in which there is no change in the internal conformation of the molecule. It is limited with monatomic molecules in the NVT ensemble[47]. In the rotational MC move, the molecule moves according

to a random direction and a random angle. In rotational moves, effects of angle torsion, angle bending and bond stretching are conserved because the molecule is taken as a rigid body. Volume change is occurred in order to avoid volume fluctuations. In this move the simulation box either expands or shrinks but the center of mass do not change.

A molecule cannot be built partially or totally by using the Metropolis algorithm therefore, Configurational bias Monte Carlo (CBMC) method is a good way to build flexible, linear or branched molecules. CBMC is also used with insertion and deletion, transfer, partial regrowth, reptation and displacement moves [47].

4. SIMULATION STUDY

4.1 System

In this study, the structural characteristics, gas separation properties and structure-solubility relationship of 3,5-diaminobenzoic acid (DABA) containing polyimides (PIs) and their copolyimide were aimed to investigate via molecular simulation tools. The PIs and their copolyimide are comprised of 4,4-hexafluoroisopropylidene-diphthalic anhydride (6FDA) and 3,3',4,4'-benzophenone tetracarboxylic dianhydride (BTDA) as dianhydride and DABA as diamine. Therefore, simulations included PI matrices of 6FDA-DABA, BTDA-DABA and 6FDA/BTDA-DABA. The chemical structures of monomers are given in Figure 4.1.

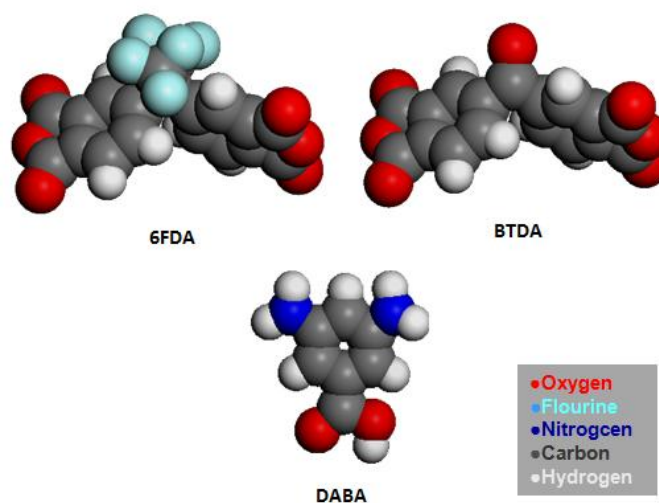


Figure. 4:1 Structures of monomers used in simulation study.

The collaboration of polar groups (-COOH) in DABA moiety leads an increase in the plasticization resistance in polyimide membranes [48] and constitutes segmental packing [49]. The functional group of 6FDA limits torsional movement of polymer chain that results increasing in free volume, thereby, permselectivity and permeability [23]. Furthermore, previous studies showed that BTDA have outstanding thermal and mechanical properties over a large range of temperatures [50]. Consequently, the structure-solubility relationships of promising polyimide and

copolyimide membranes containing 6FDA, BTDA and DABA moieties were predicted by the atomistic molecular simulation as herein described.

4.2 Methodology

All simulations were performed using the *Accelrys Materials Studio 4.1* and *5.1* software package. First, the random configurations of 6FDA-DABA, BTDA-DABA and 6FDA/BTDA-DABA matrices were generated by “*Amorphous Cell*” module. Then, the characteristic properties such as glass transition temperature (T_g), d-spacing value, cohesive energy density (CED), radius of gyration (R_g), fractional free volume (FFV), accessible free volume (AFV), and the distribution of dihedral angle of the dianhydride and diamine linkage of PI matrices were estimated using the analysis tools provided by software. Finally, in order to determine the solubility coefficients, solubility selectivities and sorption isotherms of sorbate molecules, “*Sorption*” module was used.

Intermolecular and intramolecular interactions were modeled using the COMPASS forcefield in all simulations. To estimate the van der Waals interactions atom-based calculations were used. The cutoff distance was set as the half of the lattice length of simulation box to decrease the computation time by restricting the recalculation of non-bond energies of the pairs of PI structures. The Columbic interactions were evaluated by the Ewald summation method with an accuracy of 10^{-3} . Velocity Verlet algorithm was used to integrate the equation of motion with time step of 1 fs throughout all MD runs. Both temperature and the pressure were controlled by Berendsen method. Grand Canonical Monte Carlo (GCMC) ensemble in which volume, temperature and chemical potential of the system is fixed was used in all sorption simulations.

In this section, the simulation protocols of construction and characterization of PI matrices and sorption of O_2 , N_2 , CH_4 , CO_2 , C_3H_6 and C_3H_8 in PI matrices will be explained by subheadings.

4.2.1 Construction and characterization of polyimide matrices

The first stage was the construction of the initial structures of the dianhydride and the diamine moieties, which were then optimized geometrically. Next, the repeat unit of

polymer chain was created by linking the monomer structures. To represent the real conformation of polymer chains, large system sizes were preferred. The PI chain of 6FDA-DABA consisted of 80 repeat units (4002 atoms) whereas the model for BTDA-DABA included 120 repeat units (5162 atoms). 6FDA/BTDA-DABA chain contained 80 repeat units (3862 atoms) and the ratio of 6FDA to BTDA is 3:1.

For each polyimide two different PI chains with the same number of repeat unit were constructed. The first one was constructed by setting the torsion of polymer chain to 180° and the other was constructed by setting them randomly.

PI matrices contain many rings and side groups which may result producing ring catenations and spearing in PI chain during the packing process. Therefore in order to eliminate these potential problems the structures were gradually compressed that the density was ramped up from 0.1 g/cm^3 to target density and 10 to 250 methanol molecules were added randomly into the simulation box. After reaching the target density, additional molecules were removed and to adjust the coordinates and the cell parameter of PI matrix, minimization of the models were performed. To obtain optimized density the packed models were subjected some compression and annealing procedure which is provided by Heuchel et al. [51]:

- The compression was run for 5 ps at 5000 bar via NPT-MD.
- The annealing was run for 20 ps at 600 K and then at 300 K via NVT-MD.
- An NPT-MD simulation was performed for 20 ps at 308 K and 1 bar to check packing stability. After that run, the density differs from the actual one by more than 20 %. In this case, prior compression and annealing simulations should be repeated until the difference reaches to 6%.
- Finally, for data production 300 ps MD simulation was run in an NPT ensemble at 308 K and 1 bar.

The structural properties of constructed simulation cells were estimated by using appropriate modules and tools that software provides. These structural properties consist of radius of gyration, d-spacing, cohesive energy density, fractional free volume, backbone rigidity, and the glass transition temperature.

The distance between the parallel lattice planes of polymer chains (d spacing) was determined from x-ray scattering pattern and calculated by using Bragg's equation [52].

$$n\lambda = 2d \sin \theta \tag{4.1}$$

where n is the order of a reflection, λ is the wavelength, d is d-spacing, and θ is the angle between the incident beam and a lattice plane known as the Bragg angle. The x-ray analyses were obtained as a function of the scattering vector ($1/\text{\AA}$) which can be converted to the scattering angle (2θ) through the Eq.4.2.

$$\phi = \frac{4\pi \sin \theta}{\lambda} \quad (4.2)$$

Radius of gyration (R_g) describes the overall spread of the molecule and is defined as the root mean square distance of the collection of atoms from their common center of gravity. It shows the chain configuration and the distance where polymer matrix packed firmly. R_g is formulated as,

$$R_g^2 = \frac{\sum_{i=1}^N m_i s_i^2}{\sum_{i=1}^N m_i} \quad (4.3)$$

where m_i is the mass of atom i , s_i is the distance of atom i from the center of mass, and N is the total number of atoms.

The cohesive energy is defined as the increase in energy per mole of a material if all intermolecular forces are eliminated. The CED corresponds to the cohesive energy per unit volume. When calculating the cohesive energy density for a simulated polymer, it is important to take the non-bond potential into account. So CED can be represented as:

$$CED = \frac{|E_{PBC} - E_{non-PBC}|}{V} \quad (4.4)$$

where E_{PBC} denotes energy calculated with periodic boundary, $E_{non-PBC}$ denotes energy calculated without periodic boundary and V is the volume of the system.

The fractional free volume of PI matrices were calculated from the following equation:

$$FFV = (V_T - V_0)/V_T \quad (4.5)$$

where V_T is the specific volume of a polymer at temperature T . V_0 is the volume occupied by the polymer chains and it is calculated from the van der Waals volume (V_w) [53].

$$V_0 = 1.3V_w \quad (4.6)$$

The rigidity of polymer backbone was estimated from the torsion distribution of the linkage between the functional groups of dianhydride and diamine.

The glass transition temperature (T_g) was determined by the volume change of PI matrix as a function of temperature. The system volume was procured through a series of subsequent MD runs in the NPT ensemble in which temperature varied from 700 to 450 K with 25 K cooling rate. At each temperature, the system was equilibrated two times by 50 ps runs and the average volume was obtained from the last 50 ps production. Volume and corresponding temperature were fitted as a straight line. The T_g was the intercept point of two straight lines that have different slopes (Figure 4.2). The polyimide chain in glassy state has low mobility and unrelaxed volume thus the volume change in this state is low whereas in rubbery state the polyimide has mobile chain and relaxed volume thus the volume change is high.

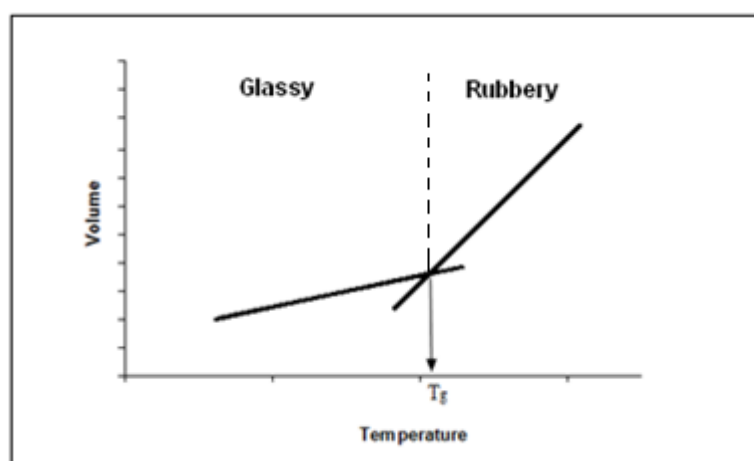


Figure 4.2: Polyimide volume as a function of temperature.

4.2.2 Sorption in polyimide matrices

The sorption behaviour of O_2 , N_2 , CH_4 , CO_2 as well as C_3H_6 and C_3H_8 on the PI matrices were predicted. The sorption simulations were accomplished by using “*Sorption*” module, which allows simulating the sorption of a pure sorbate or mixture of sorbates in a sorbent framework.

In real sorption experiments, the equilibrium of system between the sorbate and the sorbent is reached when the temperature and the chemical potentials are equal [47]. Therefore, to determine equilibrium concentration inside the PI matrices only the

temperature and the chemical potential in gas molecules have to be known. This is possible only with employing GCMC ensemble in which temperature and chemical potential of the system is fixed and the number of particles can be fluctuated during the simulation.

Depending on the structure of sorbate molecules, two different Monte Carlo algorithms were used. While Metropolis algorithm was used for the sorption of small gases (CO₂, CH₄, N₂, O₂), for hydrocarbons Configurational Bias algorithm was preferred. The structures of small gases are rigid so Metropolis algorithm in which only body translations and reorientations are introduced is proper for sorption calculations. However, hydrocarbons are large and flexible structures so configurational bias algorithm that includes torsional degrees of freedom as well as translations and reorientations is useful than Metropolis algorithm.

Simulation conditions for sorption were chosen from the literature. While simulations for CO₂ and CH₄ were carried out at 35°C and 10 atm pressure, N₂ and O₂ sorption were performed at 35°C and 2 atm pressure. In addition, the sorption simulations of hydrocarbons were performed at 50 °C and 2 atm pressure. The software allows sorption simulations by using fugacity values thus pressure values were converted to fugacity for each gas.

CO₂, propylene and propane are condensed gases thus they tend to plasticize polymeric membranes. In consequence of polymer swelling, plasticization happens. To reproduce the plasticization effects of CO₂, C₃H₆ and C₃H₈, sorption-relaxation cycles were applied until the concentrations of those molecules converged to each other. At every single cycle, the polymer matrix was loaded with sorbate molecules corresponding to its equilibrium capacity at the considered pressure, and then *NPT-MD* simulation runs were applied for 40 to 200 ps to obtain an equilibrated matrix. Next, the sorbate molecules were removed and the cycle was repeated.

Solubility coefficient (S_i) is the ratio of the volume of sorbed molecule at standard temperature and pressure (STP) to the volume of the polymer and the pressure. It was calculated by the following formula:

$$S_i = \frac{V_{sorbate}}{V_{PI\ matrix} \times P} = \frac{\frac{N_{sorbate}}{N_A} \times V_{sorbate(STP)}}{V_{PI\ matrix} \times P} \quad (4.7)$$

where;

V_{sorbate} ; total volume of sorbate gas (cm^3)

N_{sorbate} ; the number of sorbate gas (molecule)

N_A ; Avogadro's number (6.02×10^{23} molecule/mol)

$V_{\text{sorbate (STP)}}$; the molar volume of gas molecules at standard temperature and pressure ($22400 \text{ cm}^3/\text{mol}$)

$V_{\text{PI matrix}}$; volume of the PI matrix (cm^3)

P; pressure (atm)

The sorption isotherms for CH_4 , N_2 , and O_2 in polyimide matrices were performed from a series of fixed pressure simulations at different pressures.

To determine the ideal sorption selectivity in PI matrices, binary gas mixtures (CO_2/CH_4 , $\text{C}_3\text{H}_6/\text{C}_3\text{H}_8$ and O_2/N_2) were considered. The partial pressures were calculated by setting the percentages of CO_2/CH_4 , $\text{C}_3\text{H}_6/\text{C}_3\text{H}_8$ and O_2/N_2 50-50%, 50-50% and 21-79, respectively.

Finally, in order to provide a microscopic picture of the local interatomic environment between sorbates and PI matrices, radial distribution analyses of CO_2 loaded PI matrices and accessible free volume distribution analyses of CO_2 , CO_2/CH_4 , C_3H_6 , C_3H_8 and $\text{C}_3\text{H}_6/\text{C}_3\text{H}_8$ loaded PI systems were carried out.

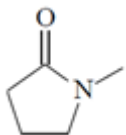
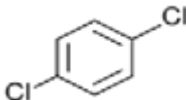
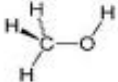
5. EXPERIMENTAL STUDY

5.1 Materials

In polyimide synthesis, in order to control the molecular weight some critical precautions and requirements should be employed. Achieving high molecular weight polyimide is possible when high purity monomers, anhydrous solvents, and dry equipment are used during the synthesis. In order to fulfill these important requirements, monomers were purified and dried in a vacuum oven, while solvents were dehydrated, and glassware was dried and purged with N₂ before charging with solvents and monomers.

The purity levels of solvents were greater than 99.5 % so they were used without preliminary purification. Properties and chemical structures of solvents are given in Table 5.1.

Table 5.1: Properties of the solvents used in the synthesis of polyimide.

	1-Methyl-2-Pyrrolidinone (NMP)	1,4-Dichlorobenzene (DCB)	Methanol (MeOH)
Supplier	Reidel-de Haën	Merck	Merck
Empirical Formula	C ₅ H ₉ NO	C ₆ H ₄ Cl ₂	CH ₄ O
Molecular Weight (g/mol)	99.13	147.00	32.04
Density (g/ml) (20°C)	1.031	1.306	0.791
Boiling point (°C)	204.3°C / 760 mmHg	174°C / 760 mmHg	64.7°C / 760 mmHg
Purity	>99.5 %	>98 %	99.9 %
Structure			

1-Methyl-2-Pyrrolidinone (NMP) was the major solvent used in the synthesis of polyimide. Due to its hygroscopic feature, this solvent was dehydrated by using 4A molecular sieves and then was sealed with a glass stopper.

1,4-Dichlorobenzene (DCB) was used during imidization to form an azeotrope with water, which should be removed from the reaction medium subsequently. DCB was dehydrated by using 4A molecular sieves and then was sealed with a glass stopper.

Methanol (meOH) was used for precipitating polyimide from NMP and DCB.

Properties of the monomers 3,3',4,4'-Benzophenone tetracarboxylic dianhydride (BTDA) and 3,5- Diaminobenzoic acid (DABA) are summarized in Table 5.2.

BTDA was used as received without further purification with a purity level of >97%. It was vacuum dried at 105 °C for 3 days prior to use in the synthesis.

DABA was purified by recrystallization from water, which is described in the next section. Prior to use, purified DABA was vacuum dried at 50 °C for 5 days.

Table 5.2: Properties of the monomers used in the polyimide synthesis.

	3,3',4,4'-Benzophenone tetracarboxylic dianhydride (BTDA)	3,5- Diaminobenzoic acid (DABA)
Supplier	Merck	Fluka
Empirical Formula	C ₁₇ H ₆ O ₇	C ₇ H ₈ N ₂ O ₂
Molecular Weight (g/mol)	322.23	152.15
Melting point (°C)	220-223	195-198
Purity	>97 %	> = 90 %

5.2 Monomer Purification

Due to the oxidation of amino groups, DABA was recrystallized from water according to following procedure [54]:

- 100 ml three necked round-bottom flask was employed as glassware. Then a condenser was inserted on the middle neck, a septum, through which N₂ purges and a thermocouple was introduced, was inserted into other neck and a rubber stopper was inserted into the last neck of the flask.
- Distilled water was boiled in another flask.
- DABA to be purified added to the three necked round-bottom flask.

- ~ 20 ml hot water per gram of DABA, which is an appropriate amount for complete dissolution of monomer, was added to the flask.
- The solution was heated up to ~95°C.
- The dissolved hot solution was poured first into heated syringe, which has 0.2 µm filter, and then into the new flask through that 0.2 µm filter.
- The solution was allowed to cool slowly and then was put under ice for 1 hour.
- To recover crystals, the solution was filtered on cold filter paper.

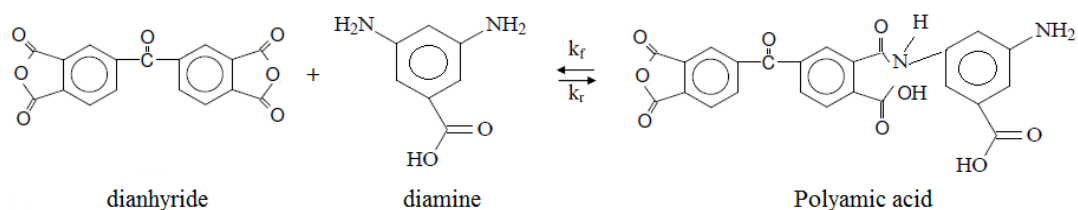
This recrystallization procedure was repeated until the filtrate was minimized and beige color DABA was obtained. The purified DABA was vacuum dried at low temperatures and was stored in a sealed dark colored glass bottle.

5.3 Polyimide Synthesis

The synthesis of polyimide is a step polymerization and is proceeding according to the principle of condensation reaction. The procedure of synthesis of polyimides has been described in the literature [55].

In this study, BTDA-DABA was synthesized via two-step reaction by one-pot rule. At the first step, poly (amic acid) was derived in an aprotic solvent from the reaction of equimolar amount of diamine and dianhydride. The nucleophilic attack of the amino group on the carbonyl carbon of the anhydride group leads to the formation of the poly (amic acid). At the second step, –OH from the acid group and –H from amine group of poly (amic acid) were removed as water from the reaction medium by closing the ring structure of poly (amic acid) then chemically stable polyimide was formed (Figure 5.1).

Step 1: Poly(amic acid) formation



Step 2: Ring Closure

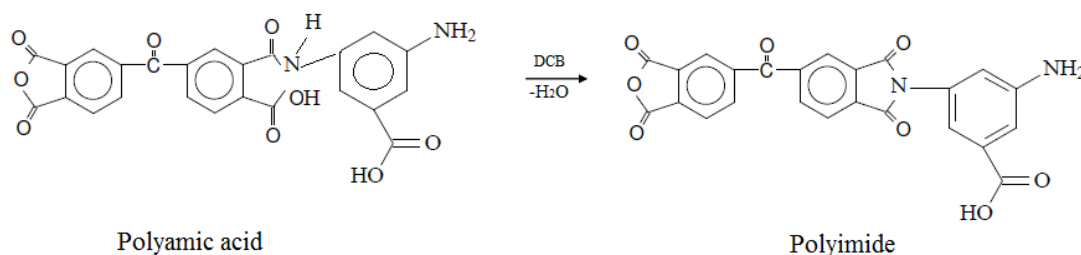


Figure 5.1: Two step condensation reaction for polyimide synthesis.

First, equimolar amounts of BTDA and DABA monomers were weighed. Poly (amic acid) formation was carried out at room temperature by first charging a 100ml three-necked round bottom flask, through which N_2 purged, with the DABA, NMP and a stir bar. After DABA was dissolved in the solvent, the BTDA was added portionwise to the flask. Equilibrium considerations needs higher concentrations, but the viscosity of solution limits the reaction kinetics if the concentration is too high [54] therefore the amount of NMP was adjusted such that the monomer concentration in the reaction solution was 15 % by weight. The conversion of the dianhydride and diamine to the desired poly (amic acid) proceeded with continuous stirring for 48 hours at ambient temperature.

After 48 hours, when poly (amic acid) formation was completed, the Dean-Stark trap and a condenser were inserted to the three-necked round bottom flask (Figure 5.2). Then DCB was added to the reaction medium. The molar ratio of NMP to DCB was 4:1. After stirring this solution for 24 hours with a nitrogen purge at $180^\circ C$ the polyimide was formed. During cyclodehydration of the poly (amic acid) water was formed in the reaction medium and it was removed with the Dean-Stark trap and condenser by forming an azeotrope with DCB. In order to maintain a constant solvent volume in the reaction medium, DCB that is removed during azeotrope was refilled by using Dean-Stark trap.

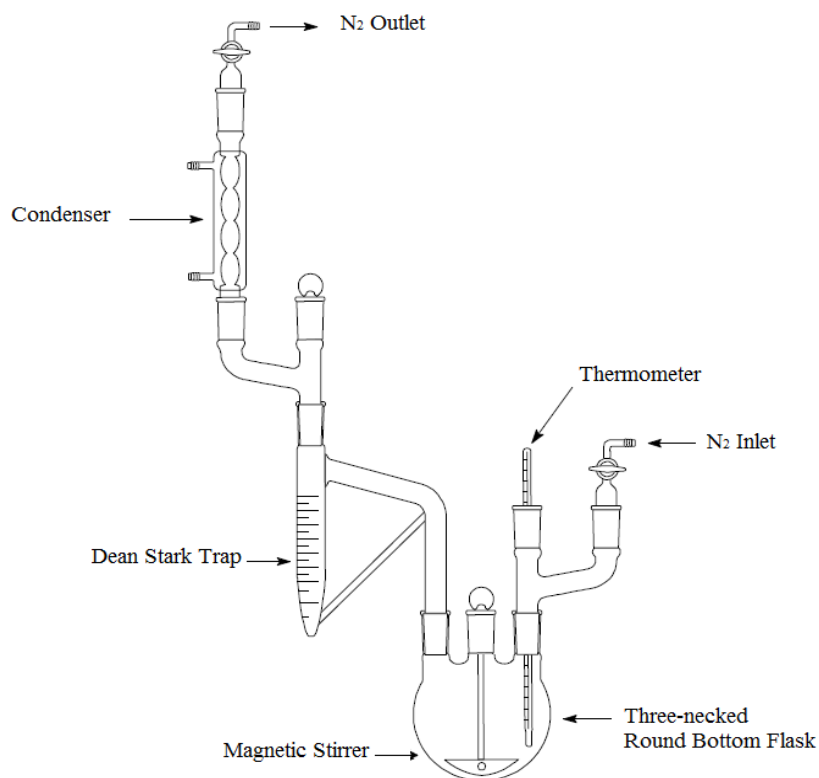


Figure 5.2: Equipment set-up for the polyimide synthesis adapted from Ref. [56].

After imidization, the solution was cooled and then precipitated out of the solution of NMP and DCB by using methanol and the recovered precipitate was dried at first 80°C for 24 hours and then 150°C in a vacuum oven for another 24 hours. The resultant polyimide was stored in dark-colored glass bottle in desiccator.

During the poly (amic acid) formation, presence of water is a considerable problem. If water hydrolyzed dianhydride, the stoichiometry is altered and high molecular weight polymer cannot be formed. To eliminate such issues following precautions should be taken:

- All glassware including reactor should be dried
- Prior to introduce diamine, N₂ should pass through the reactor
- The employed solvents which have hygroscopic feature should be dehydrated
- Monomers should be dried in vacuum oven prior to use. Synthesis process should not be started until it is ensured that diamines, which are highly hydrophilic, are dry.

- The weighing procedure of monomers and solvents should be done very quickly by using covered weighing bottle so that air contact of chemicals can be shortened as much as possible.

Moreover, monomers are sensitive chemicals. Therefore, in order to keep their purity level high, they should not be exposed to air or light for a long time. The reactor should be wrapped with foil paper during the synthesis of polyimide to eliminate the effect of light; otherwise, chain fragmentations and side reactions may take place.

5.4 Characterization of Polyimide

Various experimental techniques were used to characterize the synthesized polyimide structure. In this section, those characterization techniques with employed equipments and experimental conditions were described.

5.4.1 Fourier transform infrared spectroscopy (FTIR)

During the synthesis, key functional groups of polyamic acid and polyimide were quantitatively identified by employing Perkin-Elmer Spectrum One Fourier Transform Infrared (FTIR) Spectroscopy. Formation of functional groups of polyamic acid, such that NH-C groups, aliphatic groups and -COOH were identified at 3500 cm^{-1} , $2840\text{-}3180\text{ cm}^{-1}$, and 1670 cm^{-1} , respectively. The formation of polyimide structure was observed from aromatic imide peaks at 1780 cm^{-1} , 1720 cm^{-1} , and 1350 cm^{-1} . Furthermore, the formation of by-products such as iso-imides, anhydrides, and amines were controlled at $921\text{-}934\text{ cm}^{-1}$, 1820 cm^{-1} , and 3200 cm^{-1} , respectively.

5.4.2 Thermal gravimetric analysis (TGA)

Thermal stability, sample purity, and water content of polyimide were determined using Perkin-Elmer Thermal Gravimetric Analysis (TGA) instrument. In TGA, a sensitive balance is used to observe the weight change of a polymer as a function of temperature. Experimental runs were done at 20°C per minute heating rate from 50°C to 550°C under nitrogen purge.

5.4.3 Differential scanning calorimetry (DSC)

The glass transition temperature (T_g) of the polyimide was measured using a Perkin-Elmer Differential Scanning Calorimetry (DSC) 4000 instrument. DSC measures the difference in heat absorbed or released by a sample, as compared to an inert reference, as both are heated, cooled or held at constant temperature. During the heating process, the polymer will absorb a large amount of heat if glass transition occurs, and then the instrument keeps the temperature constant by augmenting the heat flow through the pan. Experimental runs were performed with two consecutive heating–cooling cycles. The first heating was to eliminate thermal annealing history, and the second heating run was recorded for data analysis. The measurement was conducted at a heating rate of 20°C/min from room temperature to 400°C under a nitrogen purge.

5.4.4 Wide-angle x-ray diffraction (WA-XRD)

Wide-angle X-Ray diffraction (WA-XRD) was used to qualitatively determine the interchain spacing differences in polyimide. The measurements were performed at room temperature using a PANalytical X'Pert PRO diffractometer operating at 40 kV, 30 mA. The X-Ray source was nickel filtered $\text{CuK}\alpha$ radiation with 1.54 Å wavelength. The distance between the polymer chains (d spacing) was determined by using Bragg's equation (Eqn.4.1).

6. RESULTS AND DISCUSSION

In this section, simulation and experimental results are given. Simulation results include characterization of 6FDA-DABA, BTDA-DABA and 6FDA/BTDA-DABA matrices as well as their sorption behavior and structure-solubility relationships. Experimental results related to synthesized BTDA-DABA include characterization of polyimide (PI) and the comparison with simulation results.

6.1 Simulation Results

In the first part of this study, structural properties of 6FDA-DABA, BTDA-DABA and 6FDA/BTDA-DABA were estimated by using molecular simulation tools to better understand the relationship among the structural properties of the polyimides and the corresponding copolyimide. All simulations were carried out using the *Accelrys Materials Studio* software, with all molecular interactions being modeled using the COMPASS force field.

The model for 6FDA-DABA consists of 80 repeat units in one PI chain, and the lengths of the resulted lattice vector are about 37 Å. The random configuration of BTDA-DABA includes 120 repeat units with about 40 Å lattice lengths. The lattice lengths of 6FDA/BTDA-DABA, which consists of 80 repeat units, are 36 Å and the ratio of 6FDA/BTDA in copolyimide is 3:1. The selection of this ratio is based on the study of Halitoğlu et al. [4]. After varying 6FDA/BTDA ratio as 1:1, 1:3 and 3:1, they have found that the permeability coefficients of gases in 6FDA/BTDA-DABA (3:1) are higher.

6.1.1 Characterization results

In order to predict structural properties of constructed PI models, d-spacing value, fractional free volume, radius of gyration, cohesive energy density, torsional distribution and the glass transition temperature of each polyimide and copolyimide were estimated.

The d-spacing values, which show the distance between the parallel lattice planes of polymer chains, were obtained from x-ray scattering of PI matrices. Figure 6.1 and 6.2 show the x-ray patterns of 6FDA-DABA and BTDA-DABA, respectively. Config-1 is the PI matrix whose chain was constructed by fixing the torsion to 180° and config-2 refers the PI matrix that is created with random torsion.

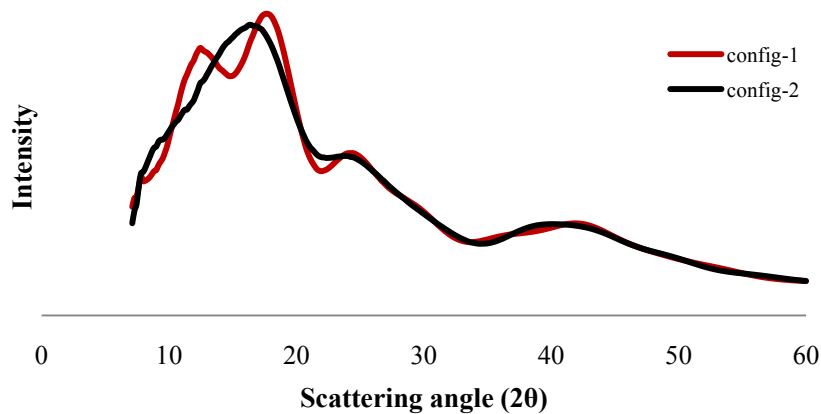


Figure 6.1: X-ray patterns of 6FDA-DABA.

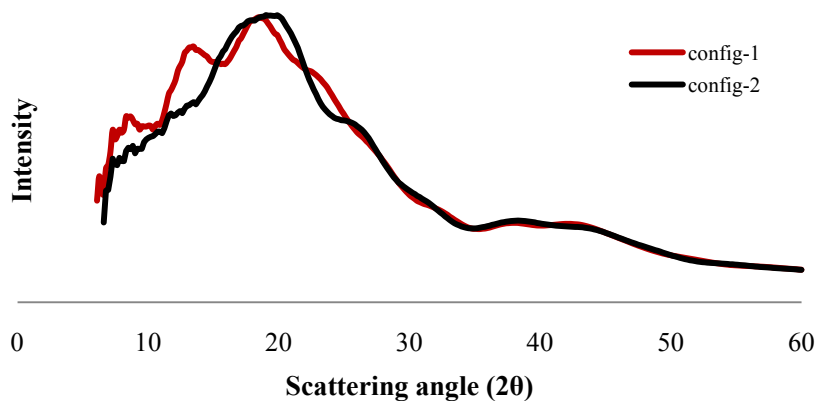


Figure 6.2: X-ray patterns of BTDA-DABA.

The first configurations of each polyimide show two sharp peaks in their x-ray pattern which means the models have 2 different d-spacing values for those configurations. However, the PI matrices that were constructed by random torsion give only a single peak and d-spacing value. The sharpest peak of first configurations presents almost at same scattering angle with the second configurations. This indicates that PI matrices that constructed by 180° torsion is more rigid than those whose torsion was set randomly. Therefore, our compression and annealing procedure for geometry optimization of DABA containing PI matrices with 180° torsion were not carried out sufficiently.

Figure 6.3 shows x-ray pattern of polyimides and copolyimide whose torsions were set randomly.

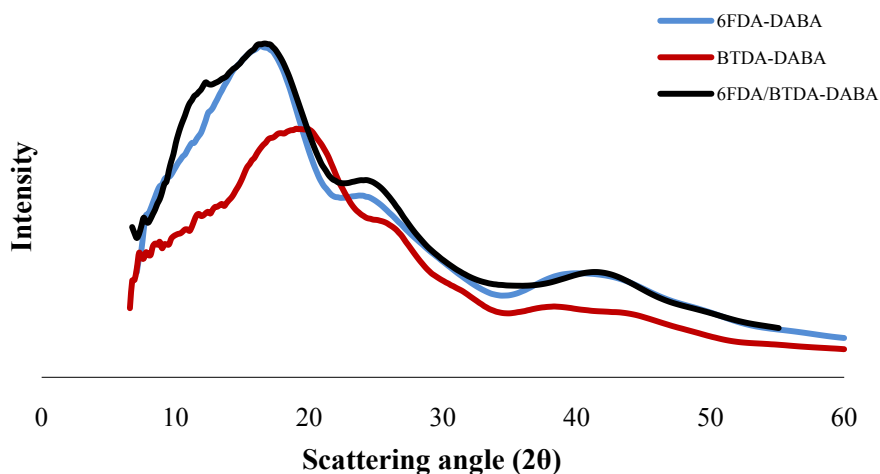


Figure 6.3: X-ray patterns of polyimides and copolyimide

X-ray patterns of 6FDA-DABA, BTDA-DABA and 6FDA/BTDA-DABA display sharp peaks at $2\theta = 16, 20$ and 17 , respectively. This scattering angles corresponds to d-spacing values of 5.37 \AA , 4.5 \AA and 5.23 \AA . Due to the bulky $-\text{C}(\text{CF}_3)_2-$ groups, 6FDA based polyimide and copolyimide display higher interchain spacings. It is obvious from the figure that 6FDA/BTDA-DABA has almost same x-ray pattern with 6FDA-DABA and its d-spacing value is in between the corresponding values of its polyimides. Although d-spacing value of 6FDA-DABA is in good agreement with the value available in the literature, d-spacing value of BTDA-DABA differs from value reported by Tsuzumi et al.[56] as presented in Table 6.1.

Fractional free volumes, cohesive energy densities, radius of gyration and glass transition temperatures are given in Table 6.1 with respect to experimental data reported in literature.

Free volume is the result of entangled polymer chains and the restriction in intermolecular interaction thus chain rotation [57]. As shown in Table 6.1 the fractional free volumes are in the order of $\text{BTDA-DABA} > \text{6FDA/BTDA-DABA} > \text{6FDA-DABA}$. This order indicates that BTDA-DABA has more rigid backbone compared to 6FDA-DABA and 6FDA/BTDA-DABA.

Cohesive energy density (CED) represents the packing properties of polymer chain. In the case of polymer chains packed closely, cohesive energy density increases. BTDA-DABA has the highest CED value, this indicates that this polyimide packed

more tightly than others. Although, the CED value of 6FDA/BTDA-DABA is between its corresponding polyimides, the values is close to 6FDA-DABA.

Table 6.1: Structural properties of 6FDA-DABA, BTDA-DABA and 6FDA/BTDA-DABA

		6FDA-DABA	BTDA-DABA	6FDA/BTDA-DABA
d-spacing (Å)	Exp	5.37 [23]	11.8-7.4 [56]	-
	Config-1	7.11-5.03	6.6-4.8	-
	Config-2	5.39	4.5	5.23
FFV	Exp	0.175 [23]	0.104 [56]	-
	Config-1	0.190	0.187	-
	Config-2	0.192	0.203	0.197
CED (Mcal/m ³)	Exp	188 [23]	267 [56]	-
	Config-1	41	50	-
	Config-2	38	64	39
R _g (Å)	Exp	-	-	-
	Config-1	19.5	23.4	-
	Config-2	19.8	24.8	19.1
T _g (°C)	Exp	348 [23]	298 [56]	-
	Config-1	348	352	-
	Config-2	346	349	380

Radius of gyration (R_g) describes the overall spread of the molecule and is used to distribute the area of PI matrix around its centroidal axis. If the concentrated area is far from the centroidal axis, PI has greater R_g value which leads resistance to bend[58]. The R_g of BTDA-DABA is around 24 Å which exceeded that value of 6FDA based polyimide and copolyimide. This result shows that BTDA-DABA resists bending which means the rigidity of this polyimide with respect to 6FDA based polyimides is higher.

In order to determine the glass transition temperatures, the volume of PI matrices that was obtained from subsequent *NPT-MD* runs was plotted as a function of temperature for both polyimides and the copolyimide (Figure 6.4-5).

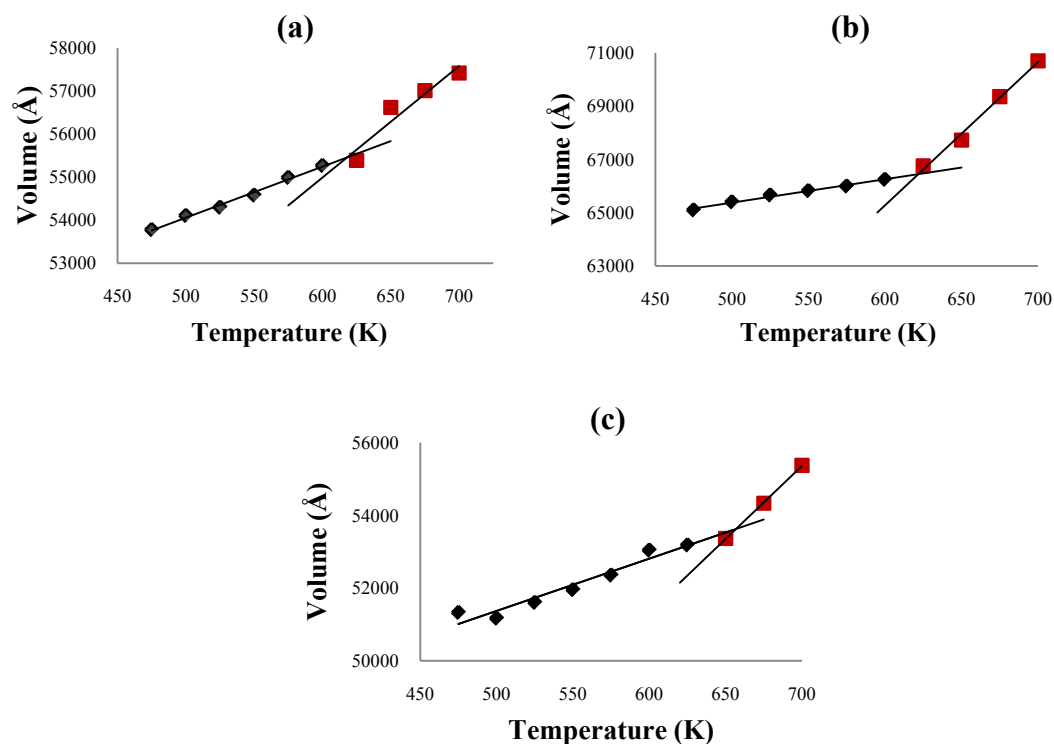


Figure 6.4: Volume of PI matrices as a function of temperature (a) 6FDA-DABA, (b) BTDA-DABA and (c) 6FDA/BTDA-DABA.

T_g value was estimated by the interception point of two straight lines with different slopes that are related to glassy and rubbery state of polyimide. The glass transitions of polyimides and copolyimide are above 300°C . Although two different models were created for 6FDA-DABA and BTDA-DABA, both configurations for each polyimides exhibit almost same glass transition temperature as shown in Table 6.1.

Even though polyimides show similar behaviors, glass transition temperature of BTDA-DABA which is 349°C is higher than that of the 6FDA-DABA that is 346°C . The glass transition temperature of aromatic polyimides is correlated with the chemical structure especially chain stiffness of the polyimide [10] thus the carbonyl-bridge of BTDA dianhydride can be suggested more rigid than the hexafluoroisopropylidene bridge of 6FDA. This result agrees the study of Wang et al. [22]. Both carbonyl and hexafluoroisopropylidene bridges restrict the rotation of 6FDA/BTDA-DABA hence in comparison with corresponding polyimides, copolyimide exhibits higher glass transition temperature at 380°C .

Like d-spacing, T_g value of 6FDA-DABA shows similarity with the experimental value that is 348 °C reported by Park et al [23]. whereas there is a discrepancy with the data for BTDA-DABA that is reported by Tsuzumi et al. [56] as 298°C.

The rigidity of PI backbones were estimated from the torsion distributions of the bridging group of dianhydrides and the linkage between amino groups of dianhydrides and diamine. Bridging groups are the carbonyl (C=O) of BTDA and the hexafluoroisopropylidene (C(CF₃)₂) of 6FDA. Figure 6.5 indicates the torsion distribution of bridging groups and it is seen that the distribution of BTDA-DABA is narrower than 6FDA-DABA. Narrow distribution is the evidence of restricted rotation thus this result confirms that carbonyl-bridge of BTDA more rigid than C(CF₃)₂ of 6FDA dianhydride.

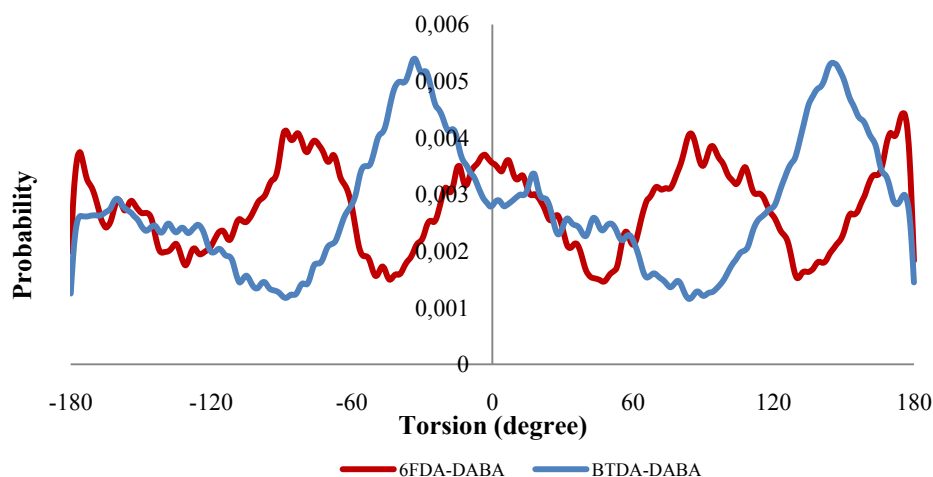


Figure 6.5: Torsion angle distribution of bridging groups of 6FDA-DABA and BTDA-DABA.

Figure 6.6 shows the torsion distribution of the linkage between amino groups of dianhydrides and diamine. It is seen that the distributions are almost same. This is because the linkage between dianhydrides and diamine of PI matrices are identical for both polyimides and copolyimide.

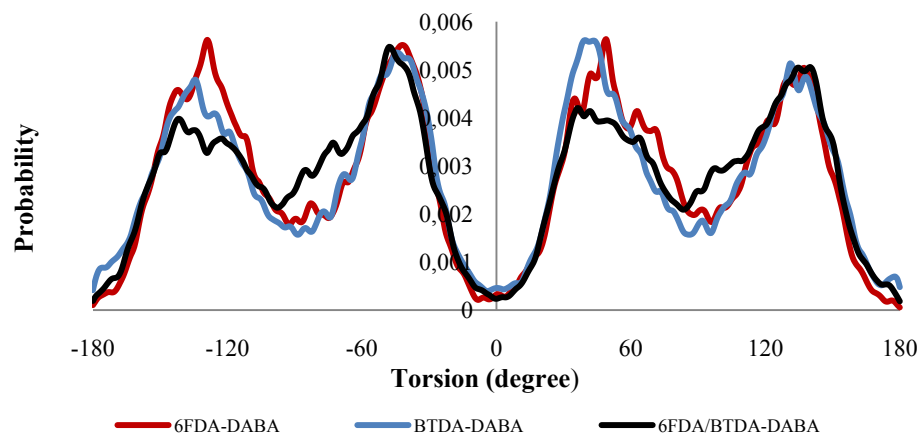


Figure 6.6: Torsion angle distribution of linkage between dianhydrides and diamine of polyimides and copolyimide.

6.1.2 Sorption results

The sorption behavior of O₂, N₂, CH₄, CO₂, C₃H₆ and C₃H₈ on the PI matrices were predicted by using Grand Canonical Monte Carlo (GCMC) simulation in which temperature and chemical potential of the system is fixed. Metropolis MC algorithm was used for the sorption of small gases (CO₂, CH₄, N₂, O₂), for hydrocarbons Configurational Bias MC algorithm was preferred. To reproduce the plasticization effects of CO₂, C₃H₆ and C₃H₈, sorption-relaxation cycles were applied until the concentrations of those molecules converged to each other.

Solubility coefficients and selectivities of pure gases as well as mixed pairs were calculated. Mixed gas simulations were performed by using partial pressures of individual gases. Partial pressures were calculated such that the gas mixture contains 21/79 % for O₂/N₂, 50/50 % for CO₂/CH₄ and 50/50 % for C₃H₆/C₃H₈.

Table 6.2 shows the solubility coefficients and selectivities of small gases in the PI matrices. For all gases, the solubilities are very close to one another in all polyimides but solubility of gases in BTDA-DABA is the highest. As mentioned in the characterization results BTDA-DABA has the highest FFV thus it has more microvoids than 6FDA-DABA and 6FDA/BTDA-DABA. It can be suggested that the introduction of carbonyl bridge in BTDA-DABA backbone enlarge the activated zone and the accessible free volume thus the gas molecules are capable to penetrate through microvoids. In other words, the increase in FFV results an increase in gas solubilities.

Both ideal and actual selectivities of gas pairs were calculated. Ideal selectivities were obtained by the ratio of corresponding solubilities. For pure gases results are similar to each other for all polyimides. But for mixed gas case, the selectivity of BTDA-DABA for CO₂/CH₄ mixture is about twice higher than 6FDA-DABA.

Table 6.2: Solubility coefficients and solubility selectivities of O₂, N₂, CO₂ and CH₄.

	S (cm ³ (STP) / cm ³ atm)				Solubility Selectivity	
	O ₂	N ₂	CO ₂	CH ₄	O ₂ /N ₂ (21:79)	CO ₂ /CH ₄ (50:50)
6FDA-DABA						
Pure	3.43	2.20	8.61	1.70	1.56	5.06
Mixed	3.59	2.07	13.00	0.58	1.74	22.41
BTDA-DABA						
Pure	4.64	2.93	10.22	1.95	1.58	4.97
Mixed	4.85	2.88	16.63	0.41	1.69	40.56
6FDA/BTDA-DABA						
Pure	4.15	2.78	9.20	2.17	1.49	4.24
Mixed	4.34	2.68	15.55	0.53	1.62	29.34

For each polyimides sorption isotherms of O₂, N₂, and CH₄ were obtained at 35°C (Figure 6.7-8). It can be seen from the figures that N₂ and CH₄ solubility behaviors of each polyimides almost same. Compared to N₂ and CH₄, O₂ can be suggested to be the most soluble gas in polyimides, however they show similar manners at low pressures.

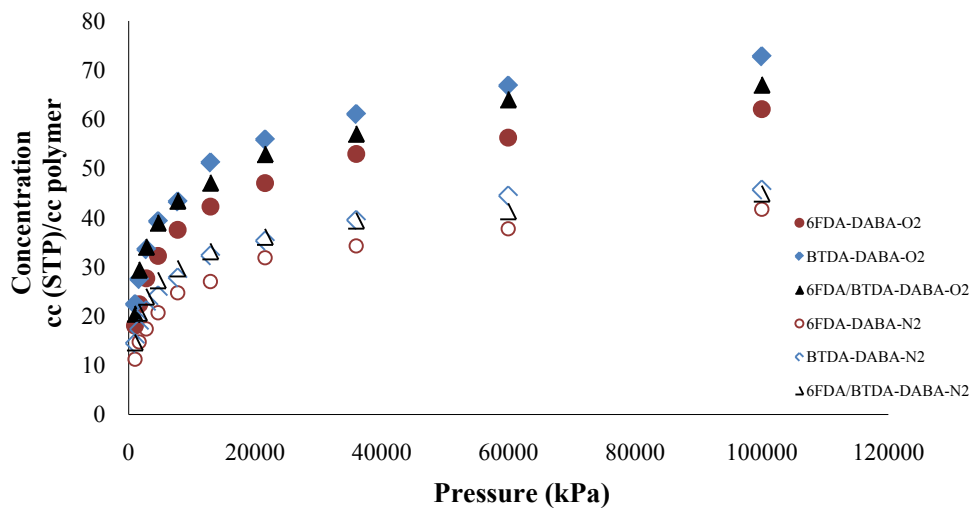


Figure 6.7: O₂ and N₂ sorption isotherms of polyimides and copolyimide at 35°C.

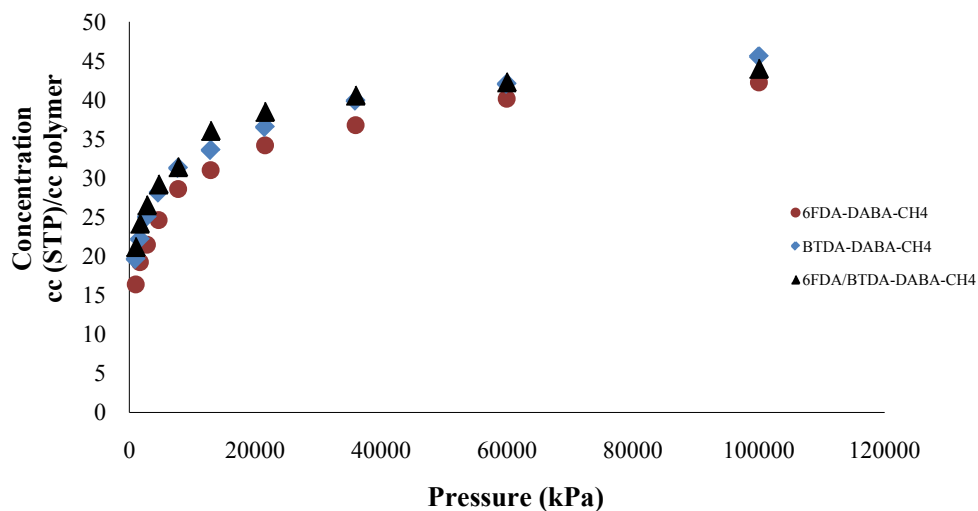


Figure 6.8: CH₄ sorption isotherms of polyimides and copolyimide at 35°C.

Table 6.3 shows the solubility coefficients and selectivities of hydrocarbons in the PI matrices at 50°C, 2 atm. With respect to its polyimides, solubility of propane and propylene of 6FDA/BTDA-DABA is the highest. However the ideal solubility selectivity of copolyimide is the lowest. Propane solubility of BTDA-DABA is about twice higher than 6FDA-DABA.

Table 6.3: Solubility coefficients and solubility selectivities of C₃H₆ and C₃H₈

	S (cm ³ (STP) / cm ³ atm)		Solubility Selectivity
	C ₃ H ₆	C ₃ H ₈	C ₃ H ₆ /C ₃ H ₈ (50:50)
6FDA-DABA			
Pure	10.88	7.16	1.53
Mixed	15.83	6.72	2.36
BTDA-DABA			
Pure	16.22	13.68	1.19
Mixed	22.83	10.17	2.24
6FDA/BTDA-DABA			
Pure	21.29	18.57	1.15
Mixed	29.09	12.39	2.35

Plasticization leads an increment in gas solubility. This is because swelling after dissolution of certain gas molecules affects chain packing thus free volume of polymer matrix is increased [17]. Table 6.4 and 6.5 present fractional free volume of polyimides after CO₂, CO₂/CH₄, C₃H₆, C₃H₈ and C₃H₆/C₃H₈ sorption. After the sorption of all gases and gas pairs, the increase in FFV of 6FDA/BTDA-DABA is the highest which means the copolyimide is the most swollen one with respect to its polyimides.

Table 6.4: Fractional free volume of the PI matrices after CO₂ and CO₂/CH₄ sorption

	Equilibrated unit cell	FFV		Increase %	
		CO ₂	CO ₂ /CH ₄	CO ₂	CO ₂ /CH ₄
6FDA-DABA	0.192	0.244	0.239	27	25
BTDA-DABA	0.203	0.268	0.245	32	21
6FDA/BTDA-DABA	0.197	0.261	0.248	32.5	26

Table 6.5: Fractional free volume of the PI matrices after C₃H₆, C₃H₈ and C₃H₆/C₃H₈ sorption

	Equilibrated unit cell	FFV			Increase %		
		C ₃ H ₆	C ₃ H ₈	C ₃ H ₆ /C ₃ H ₈	C ₃ H ₆	C ₃ H ₈	C ₃ H ₆ /C ₃ H ₈
6FDA-DABA	0.192	0.211	0.208	0.220	10	9	15
BTDA-DABA	0.203	0.231	0.230	0.238	14	13	17
6FDA/BTDA-DABA	0.197	0.252	0.264	0.263	28	34	34

Relaxation to obtain an equilibrated matrix during reproduction of the plasticization effects of CO₂, C₃H₆ and C₃H₈ were done by *NPT-MD* simulation runs for 40 to 200 ps. Figures 6.9-11 demonstrate the CO₂, C₃H₆, C₃H₈, CO₂/CH₄ and C₃H₆/C₃H₈ sorption steps of 6FDA-DABA matrix.

Relaxation of 6FDA-DABA in CO₂ and C₃H₈ plasticization was done by 40 ps simulation time whereas 200 ps runs were carried out for C₃H₆ plasticization. Short time relaxation enhances sorption steps thus the time of equilibrium of PI matrix extends. Similar results were obtained for BTDA-DABA and 6FDA/BTDA-DABA. The CO₂, C₃H₆, C₃H₈, CO₂/CH₄ and C₃H₆/C₃H₈ sorption steps of these PI matrices are presented in Appendix A.

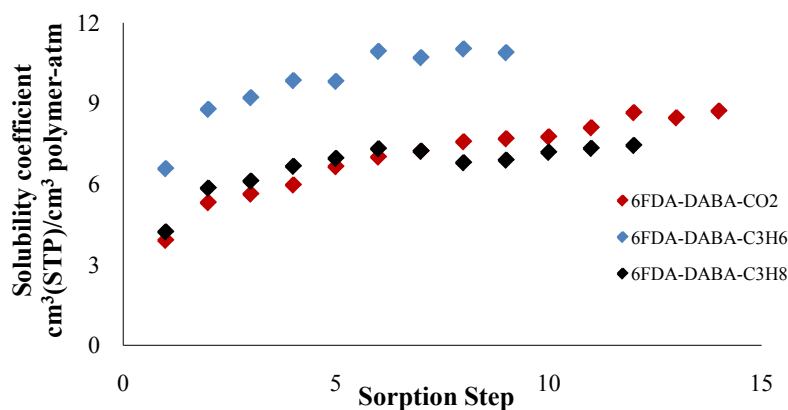


Figure 6.9: CO₂, propylene and propane sorption in 6FDA-DABA.

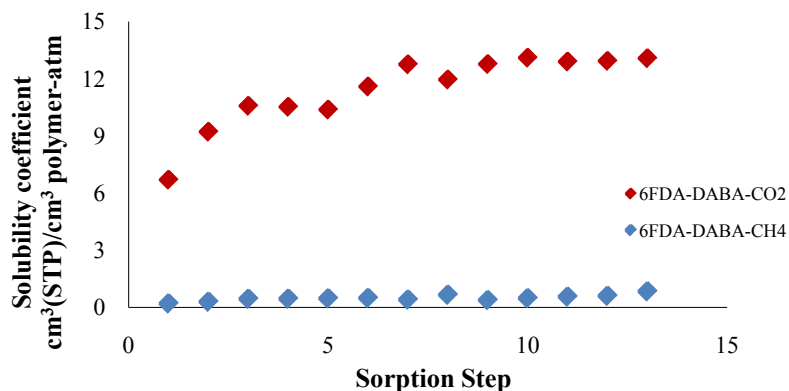


Figure 6.10: CO₂/CH₄ sorption in 6FDA-DABA.

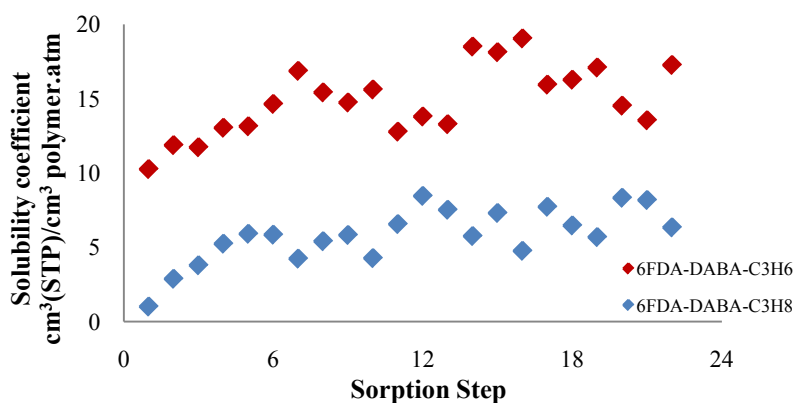


Figure 6.11: C₃H₆/C₃H₈ sorption in 6FDA-DABA.

As an effect of plasticization, which induced by both C₃H₆ and C₃H₈, the 6FDA-DABA matrix swells during the sorption. As seen from Fig. 6.11 that this effect increases the solubility of C₃H₆ while the solubility of C₃H₈ in PI matrix decreases or vice versa thus the selectivity of membrane system decreases. Similar behaviors for C₃H₆/C₃H₈ sorption in BTDA-DABA and 6FDA/BTDA-DABA matrices were observed and the results are presented in Appendix.

The percentage of accessible free volume and the probe radius in the 6FDA-DABA, BTDA-DABA and 6FDA/BTDA-DABA matrices were obtained as results of the probing test method. The accessible free volume was calculated by rolling a probe with a given radius. The reason for choosing the probing radius between 0–3.2 Å is that the kinetic radii of CO₂, CH₄, C₃H₆ and C₃H₈ are 1.65, 1.91, 2.2, and 2.3 Å [25], respectively.

Figure 6.12-14 show the accessible free volume distribution of PI and PI/sorbate systems. The available free volumes in PI matrices in the absence of sorbate molecules are distributed with radius $< 0.8 \text{ \AA}$ where the percentages of accessible free volume of empty cells are higher. An increase of the radius of the probing results in a decrease of the accessible free volume this is because gas molecules occupy free volumes that are correspond to kinetic radii of gas molecules.

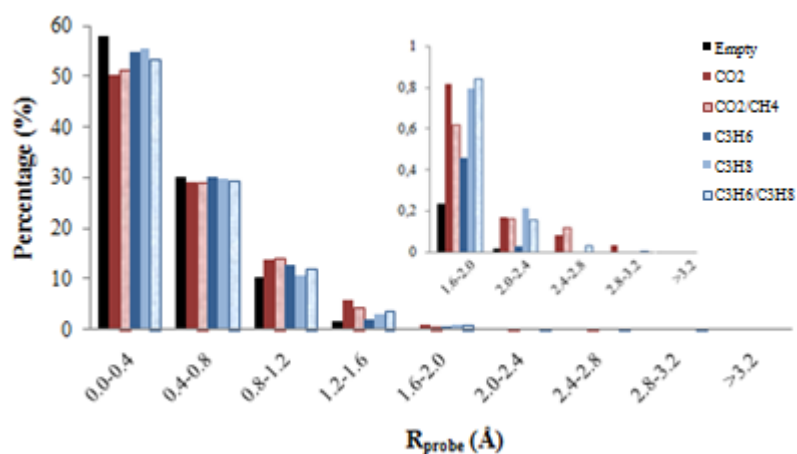


Figure 6.12: Accessible free volume distribution of 6FDA-DABA and 6FDA-DABA/sorbate systems.

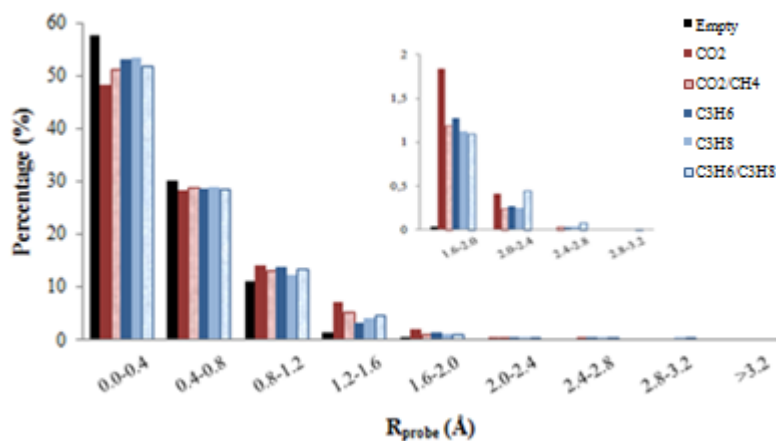


Figure 6.13: Accessible free volume distribution of BTDA-DABA and BTDA-DABA/sorbate systems.

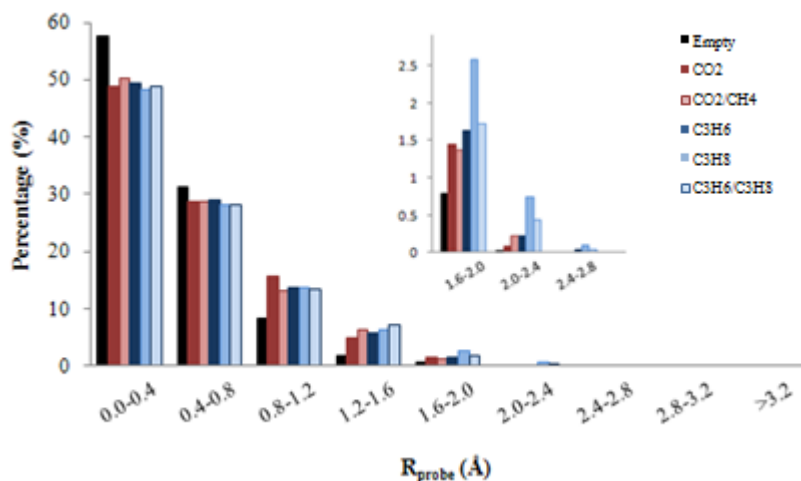


Figure 6.14: Accessible free volume distribution of 6FDA/BTDA-DABA and 6FDA/BTDA-DABA/sorbate systems.

Figure 6.15 shows the accessible free volume distribution of empty cells of polyimides and copolyimide, and also their CO₂ loaded systems. At probing radius of 1.6 Å, which is the kinetic radius of CO₂, the accessible free volume of BTDA-DABA/CO₂ system is higher. As mentioned previously, the solubility of CO₂ in BTDA-DABA matrix is the highest which means interactions between CO₂ and BTDA-DABA is the strongest, this strong interaction dilates the volume of PI matrix thus larger accessible voids appear.

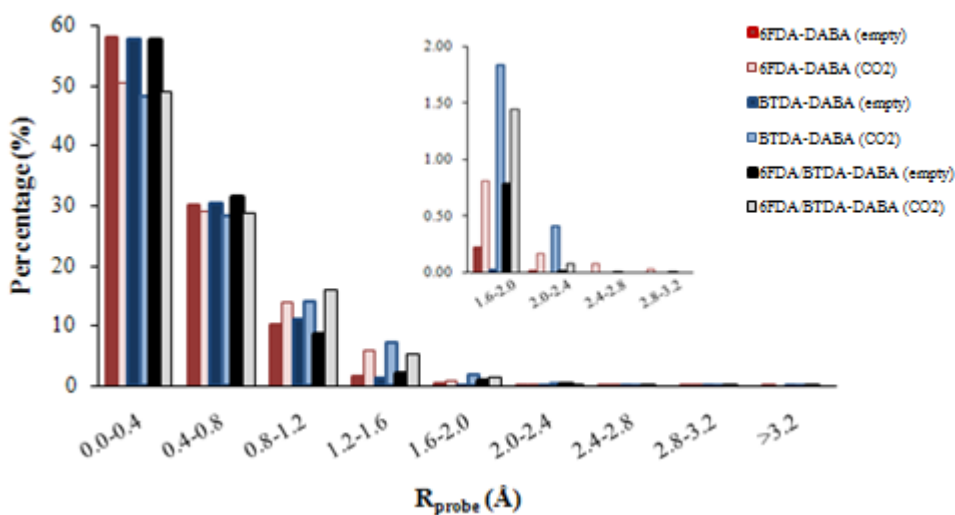


Figure 6.15: Accessible free volume distribution of polyimides/CO₂ and copolyimide/CO₂ systems.

Figure 6.16-17 show the accessible free volume distribution of empty cells of polyimides and copolyimide, and also their C_3H_6 and C_3H_8 loaded systems, respectively. At probing radius between 1.6 and 2.0 Å, accessible free volumes of 6FDA/BTDA-DABA- C_3H_6 and 6FDA/BTDA-DABA- C_3H_8 system are higher. Solubility of C_3H_6 and C_3H_8 in copolyimide is the highest and also copolyimide swelled more significant than its polyimides after C_3H_6 and C_3H_8 sorption. Therefore volume dilatation occurs in copolyimide matrix more than polyimide matrices thus more accessible voids appear for copolyimide/ C_3H_6 and copolyimide/ C_3H_8 systems.

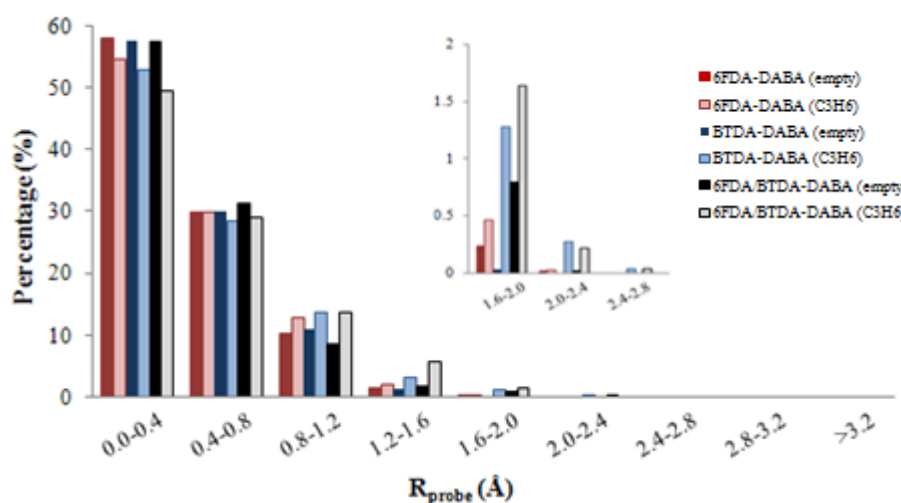


Figure 6.16: Accessible free volume distribution of polyimides/ C_3H_6 and copolyimide/ C_3H_6 systems.

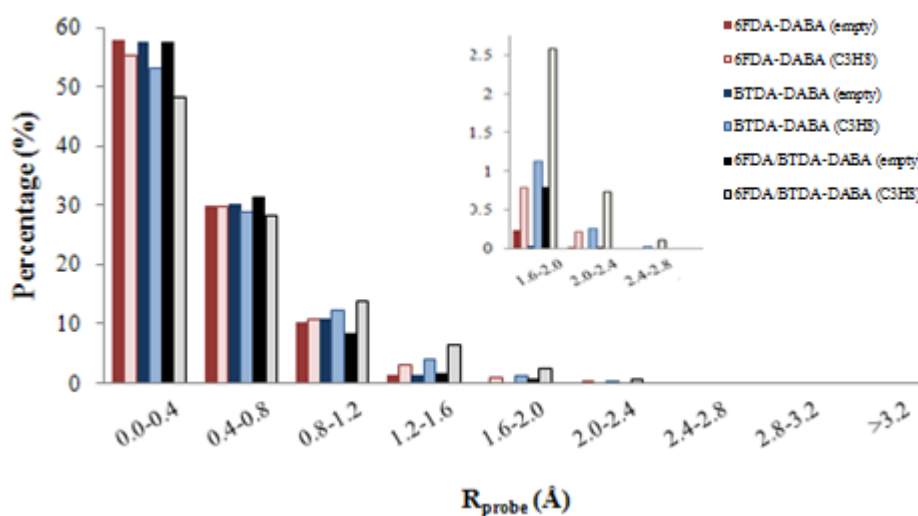


Figure 6.17: Accessible free volume distribution of polyimides/ C_3H_8 and copolyimide/ C_3H_8 systems.

In order to investigate microscopic view of the interatomic environment of CO₂ solubility in PI matrices, radial distribution analysis were performed. The radial distribution function $g(r)$ is pair correlation that describes the quantity of atomic density that varies as a function of the distance r from one particular atom with respect to the bulk phase [25].

Figure 6.18 shows one 6FDA-DABA repeat unit and the atoms, whose interactions with CO₂ were estimated. They are defined as F, N1, O1, O2 and O3. F is the fluorine in -CF₃ group of 6FDA, N1 and O1 are the nitrogen and oxygen in imide, O2 and O3 are the oxygen from carbonyl and hydroxyl group of DABA, respectively.

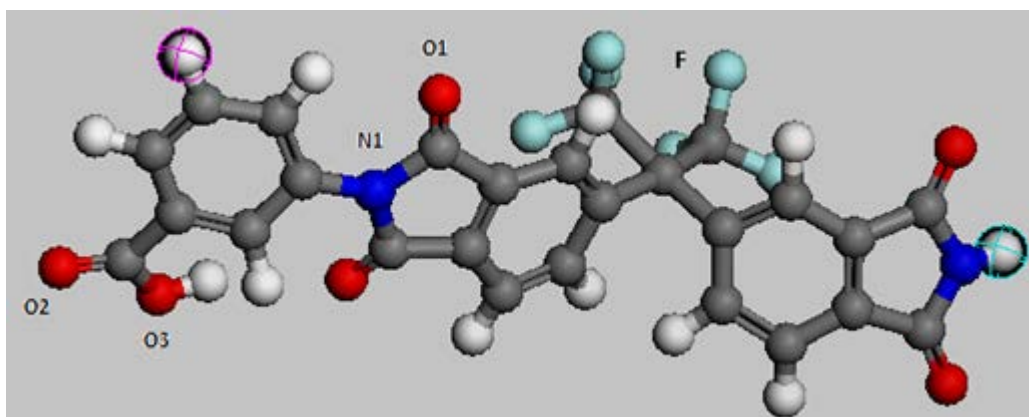


Figure 6.18: Repeat unit of 6FDA-DABA.

6FDA-DABA matrix is loaded 54 CO₂ molecules at first sorption step, after reaching the equilibrium the polyimide is loaded 128 CO₂ molecules. The number of loaded CO₂ molecules may shift the interaction sites of PI matrix. In order to account for this behavior 128 CO₂ loaded polyimide also analyzed by the radial distribution function.

Figure 6.19 shows the $g(r)$ of CO₂ around selected atoms of the 6FDA-DABA matrix. The location of peaks in $g(r)$ can be used to identify the interaction distance between gas molecules and PI matrices.

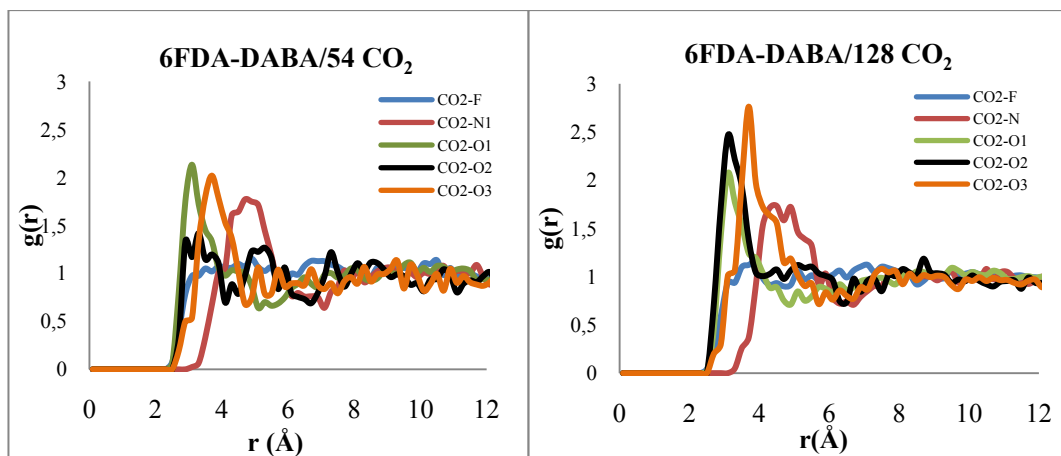


Figure 6.19: Radial distribution functions of CO₂ around F, N1, O1, O2 and O3 atoms of 6FDA-DABA.

The most distinctive peaks in the presence of 54 CO₂ molecules are seen at 3.1 Å, 3.7 Å and 4.7 Å which correspond to the $g(r)$ of CO₂-O1, CO₂-O3 and CO₂-N1, respectively. It indicates that the O1 and N1 atoms in imide and O3 atom from DABA are the preferential sorption sites for CO₂. The $g(r)$ of CO₂-F and CO₂-O2 show lower peaks which means these atoms are not accessible by CO₂ molecules. The interaction between CO₂ and F atoms is the weakest one. In the presence of 128 CO₂ molecules, distinct peaks are observed at 3.1 Å, 3.1 Å and 3.7 Å which are related to O1, O2 and O3 atoms, respectively. This shows clearly that preferential sites shift to carboxyl and hydroxyl group of DABA at high loading.

The differences between interactions at low and high loading corresponding initial and final stages of sorption are shown in Figure 6.20 for each sorption site separately. There is no pronounced change in CO₂-F and CO₂-N1. Interactions between CO₂-O2 and CO₂-O3 increase when CO₂ loading increased. The favored site that is CO₂-O1 shows no change. During loading, CO₂ occupies initially to the O1 sites of 6FDA-DABA matrix, but after a time these sites are saturated with CO₂ molecules so at high loadings these gas molecules occupy the least preferential sites like O2.

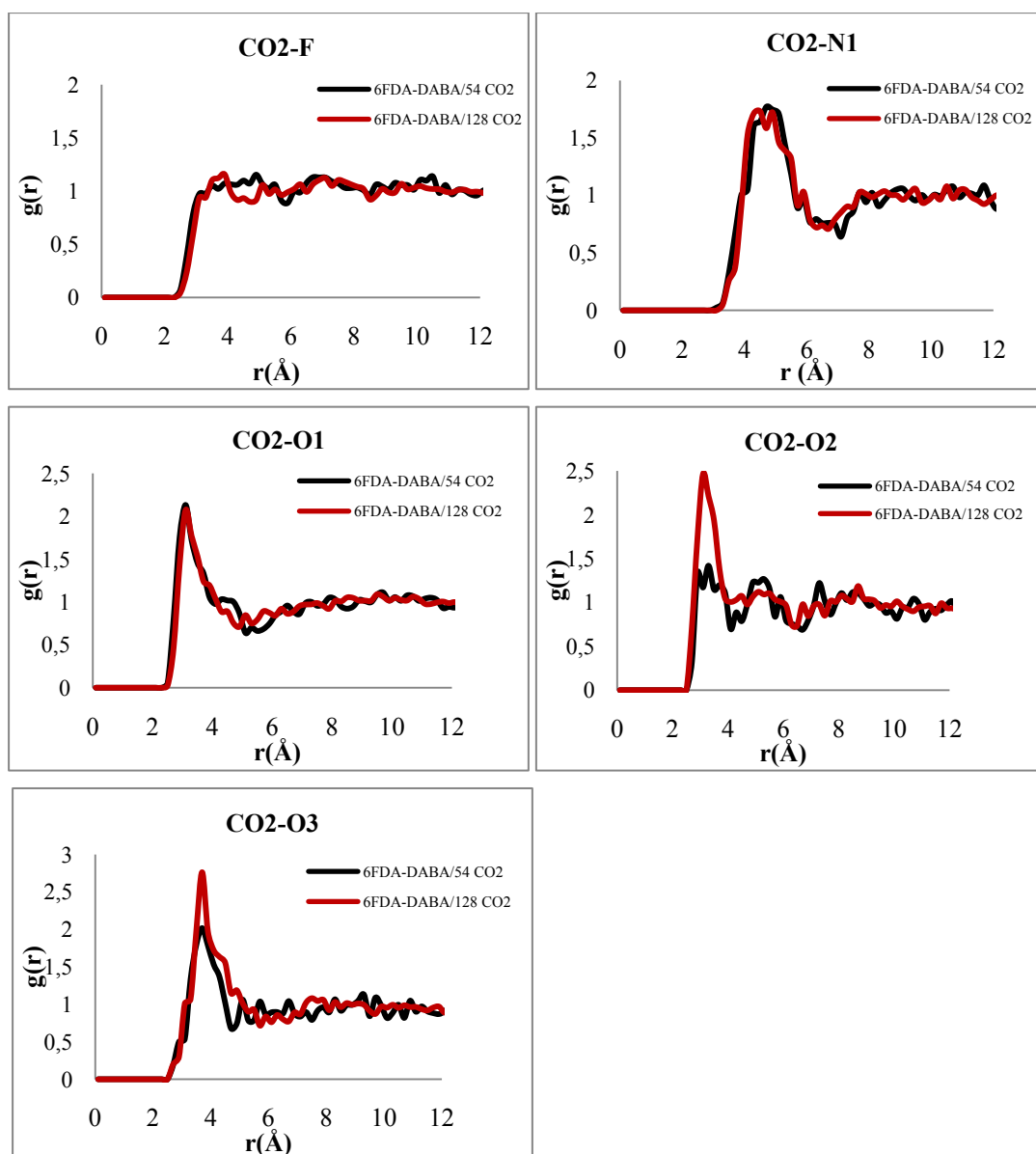


Figure 6.20: Radial distribution functions of CO₂ around F, N1, O1, O2 and O3 in 6FDA-DABA/CO₂ system at a loading of 54 and 128 CO₂.

Figure 6.21 shows one BTDA-DABA repeat unit with chosen atoms whose interactions with CO₂ were estimated. These atoms are; the nitrogen and oxygen in imide, the oxygen of carbonyl and hydroxyl group of DABA and the oxygen of carbonyl of benzophenone. They are defined as N1, O1, O2, O3 and O4.

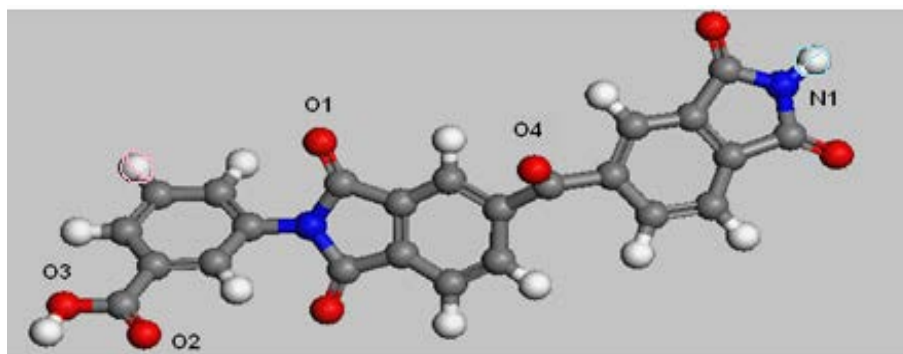


Figure 6.21: Repeat unit of BTDA-DABA.

BTDA-DABA matrix loaded 83 CO₂ molecules at first sorption step, and the polyimide loaded 198 CO₂ molecules when it reached the equilibrium after plasticization. In order to account for the change in interaction sites 198 CO₂ loaded polyimide also analyzed by radial distribution function.

Figure 6.22 shows the $g(r)$ of CO₂ around characteristic atoms of the BTDA-DABA matrix which includes 83 and 198 CO₂ molecules in simulation box. It is clearly observed in the $g(r)$ that O1, N1 and O4 show explicit peaks at 3.5 Å, 3.7 Å and 4.7 Å, respectively in the presence of 83 CO₂ molecules. Although this situation indicates that CO₂ molecules are sorbed initially by O1, N1 and O4 sites, O2 and O3 atoms also prominently interact with CO₂.

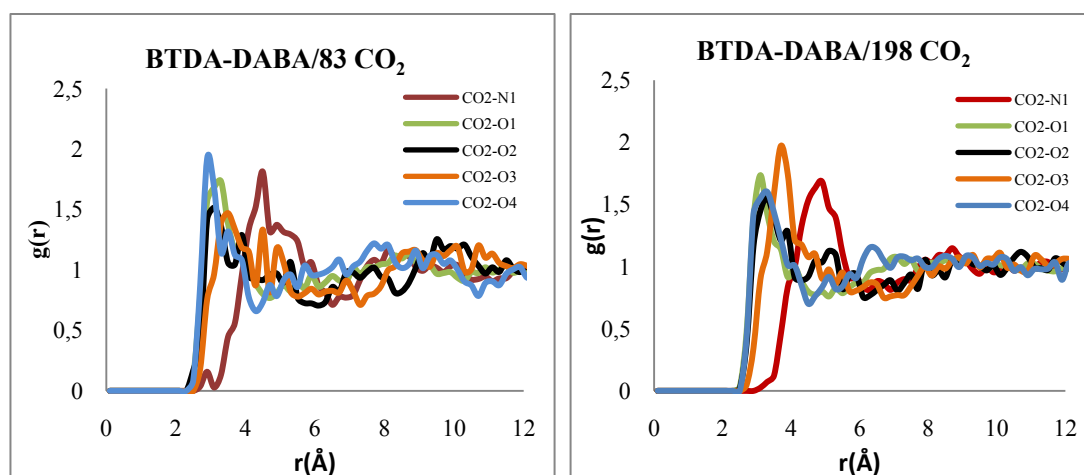


Figure 6.22: Radial distribution functions of CO₂ around N1, O1, O2, O3 and O4 atoms of BTDA-DABA.

In the presence of 198 CO₂ molecules, distinct peaks are observed at 3.7 Å which is related to O3 as shown Figure 6.22. This shows clearly that O3 sites of the PI matrix interact with CO₂ strongly than other sites.

The differences between interactions at low and high loading corresponding initial and final stages of sorption are shown in Figure 6.23 for each sorption site separately.

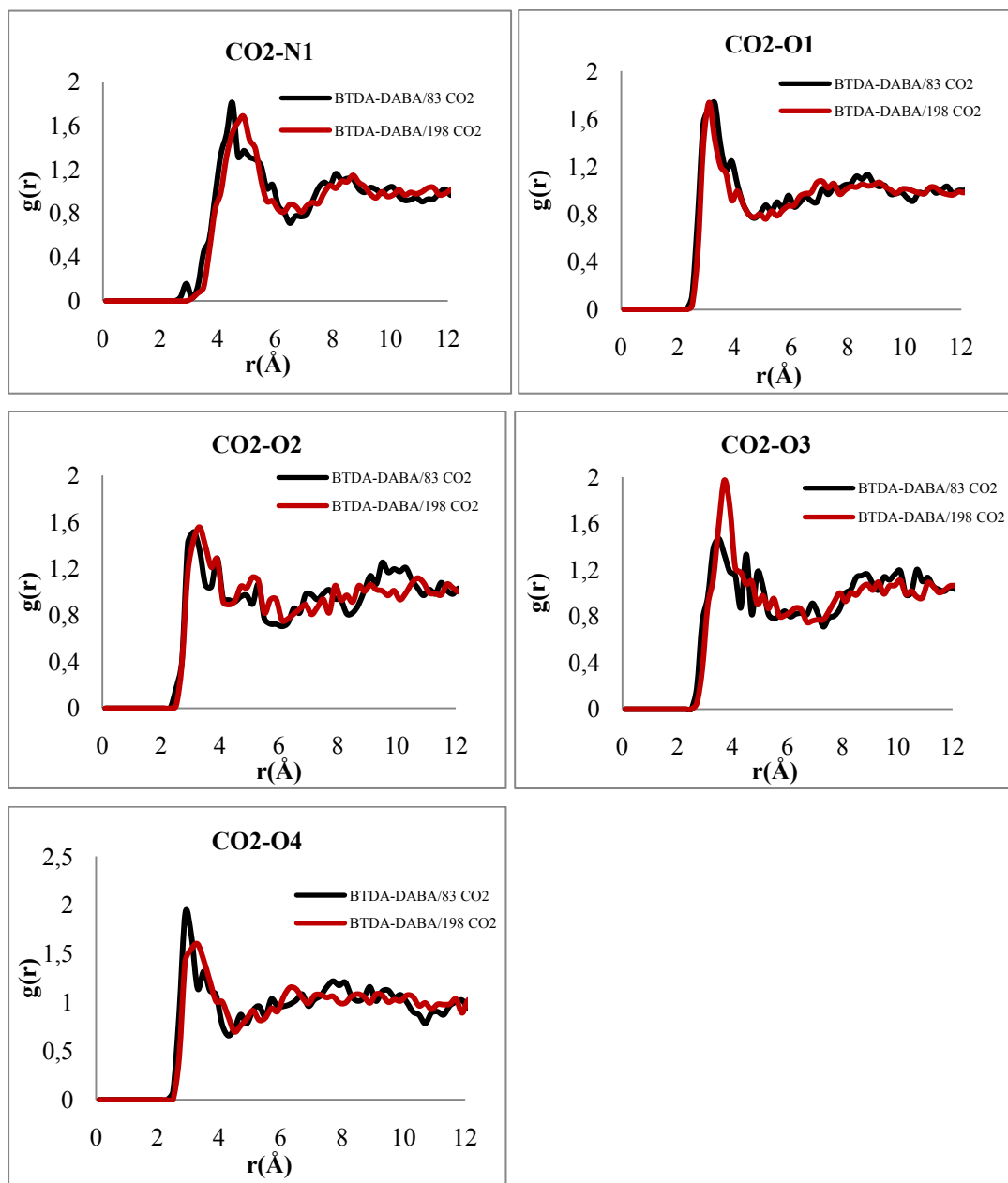


Figure 6.23: Radial distribution functions of CO₂ around N1, O1, O2, O3 and O4 in BTDA-DABA/CO₂ system at a loading of 83 and 198 CO₂.

It is obvious in figure that the peak height of CO2-N1 and CO2-O1 decrease as CO₂ loading increases from 83 to 198. This is because that O4 and N1 are strongly interacted sites, and they are fully occupied by CO₂ molecules. With increasing CO₂ loading, these sites become saturated and CO₂ starts to occupy O3 sites that are less preferential sites at low loadings. It is particularly obvious for the O3 atoms that the peak at around 4Å become sharper when the loading is increased to 198.

Repeat unit of 6FDA/BTDA-DABA with chosen atoms whose interactions with CO₂ were estimated is shown in Figure 6.24. These atoms are; the fluorine (F) in –CF₃ group of 6FDA, the nitrogen (N1, N2) and oxygen (O1, O3) in imides, the oxygen (O2) of carbonyl of benzophenone and the oxygen (O4, O5) of carbonyl and hydroxyl group of DABA.

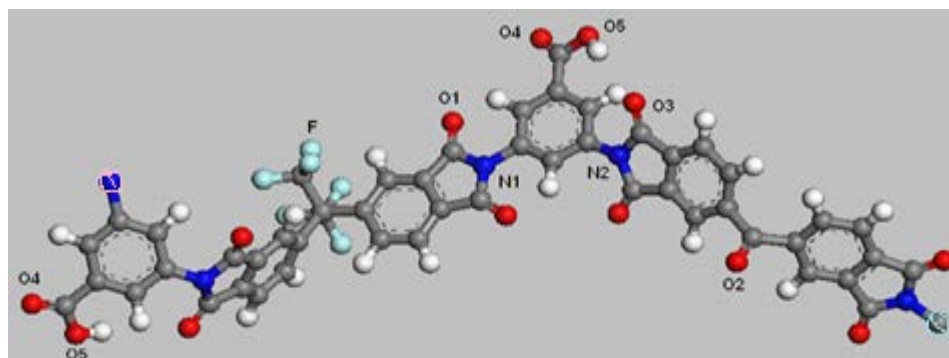


Figure 6.24: Repeat unit of 6FDA/BTDA-DABA

The $g(r)$ of CO₂ around typical atoms of the 61 CO₂ loaded 6FDA/BTDA-DABA matrix is shown in Figure 6.25.

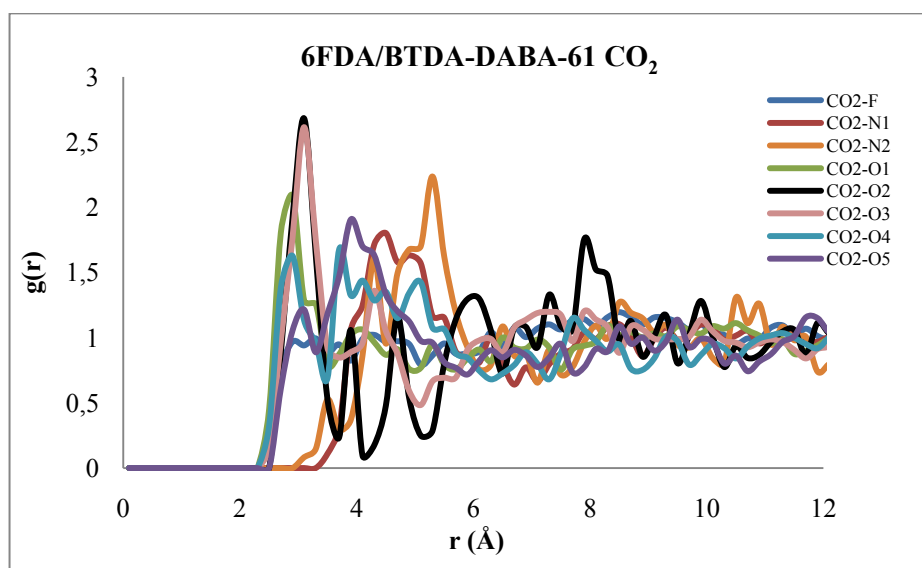


Figure 6.25: Radial distribution functions of CO₂ around F N1, N2, O1, O2, O3, O4 and O5 atoms of 6FDA/BTDA-DABA at a loading of 61 CO₂

The most distinctive peaks for 6FDA/BTDA-DABA-CO₂ system belong to the $g(r)$ of CO₂–O₂ and CO₂–O₃ both at 3.1 Å. This shows that O₂ and O₃ atoms from BTDA unit are the favorable sites for CO₂ sorption. Furthermore, CO₂-N₂ and CO₂-O₁ show pronounced peaks at 5.3 Å and 2.9 Å, respectively. The O₄, O₅ and N₁ atoms have relatively weak interactions as seen from the Fig.6.25. Likewise 6FDA-

DABA matrix, the $g(r)$ of CO₂-F shows lower peak because of limited interaction caused by the bulky -CF₃ group.

After increasing loading to 132 CO₂ molecules, the strong interactions noticeably shift to O5 and N2 sites as shown in Figure 6.26. Except for F, all atoms interact with CO₂.

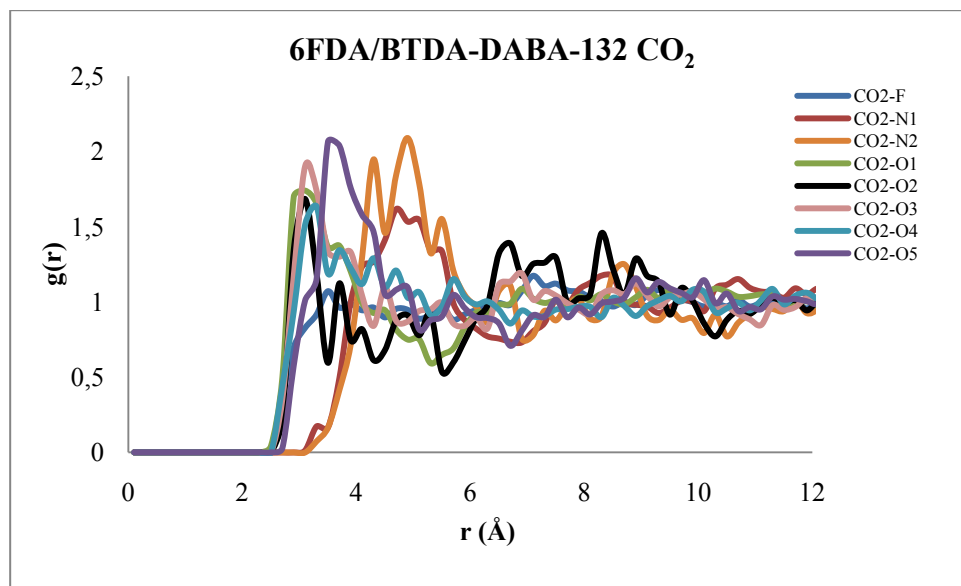


Figure 6.26: Radial distribution functions of CO₂ around F, N1, N2, O1, O2, O3, O4 and O5 atoms of 6FDA/BTDA-DABA at a loading of 132 CO₂

Individual change between the interactions of CO₂ and entire typical atoms is shown in Figure 6.27. It is obvious that the peak height of CO₂-O2 and CO₂-O3 decrease as CO₂ loading increases from 61 to 132.

The height of peaks related with CO₂-O1 diminishes depending on the loading. These are all because of that O2, O3 and also O1 are the preferential interaction sites, and they are fully occupied with CO₂ molecules. With increasing CO₂ loading, these sites become saturated and cannot interact with CO₂ molecules.

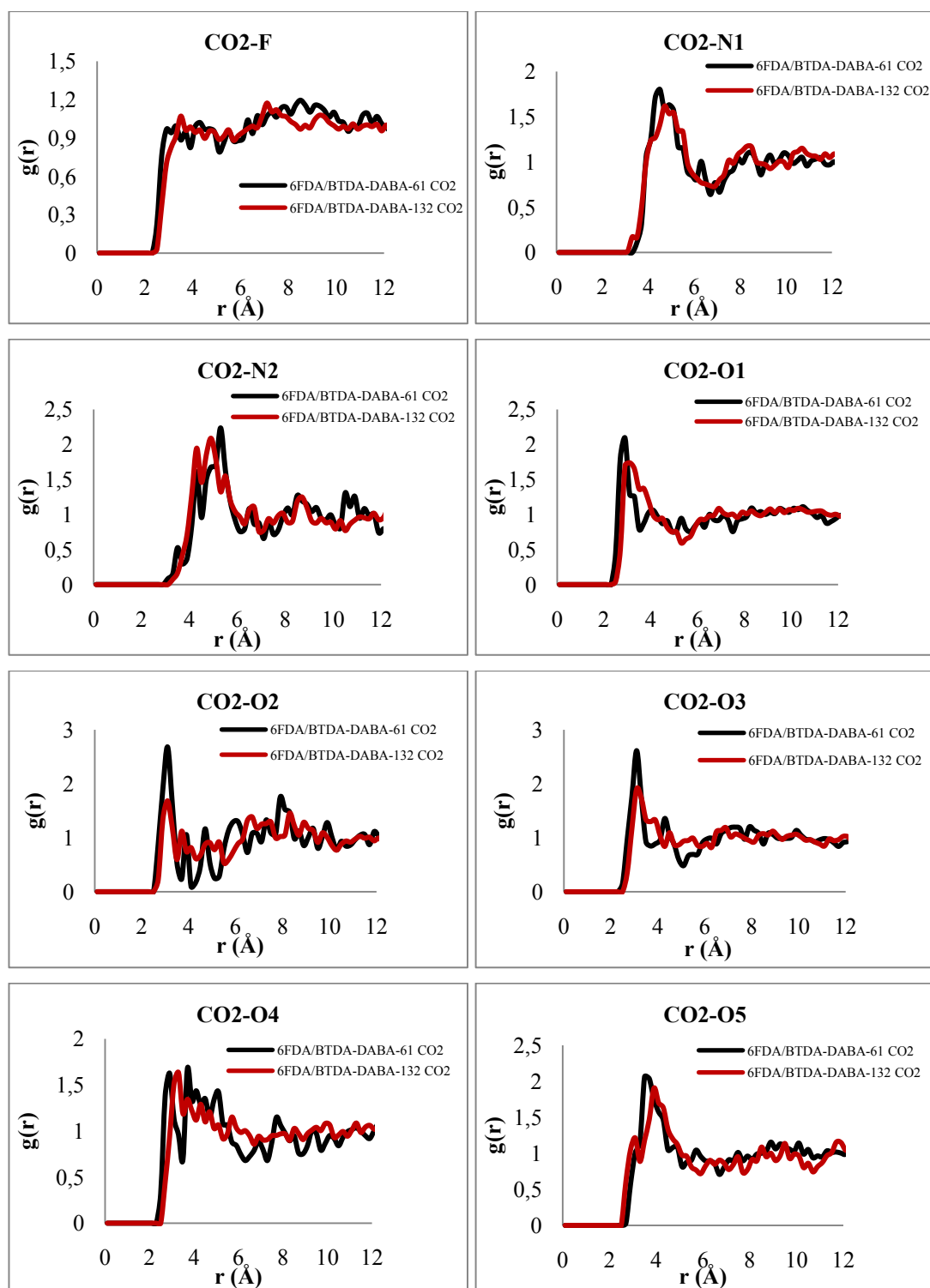


Figure 6.27: Radial distribution functions of CO₂ around F, N1, N2, O1, O2, O3, O4 and O5 in 6FDA/BTDA-DABA/CO₂ system at a loading of 61 and 132 CO₂.

6.2 Experimental Results

The glass transition temperatures (T_g) and d-spacing values of BTDA-DABA that were obtained from molecular simulation were compared with experimental data in literature. The comparison indicates that the reported T_g and d-spacing values did not match from simulation results that obtained. Due to the disagreement, the synthesis and characterization of BTDA-DABA were performed using the procedure outlined in the experimental section.

The synthesis was carried out via two-step polycondensation reaction by one-pot rule. First, equimolar amount of dianhydride and diamine react to form a poly (amic acid) solution, which is then cyclodehydrated by solution imidization to yield the polyimide. Water that is formed during cyclodehydration was removed by 1,4-dichlorobenzene (DCB).

Fourier Transform Infrared Spectroscopy (FTIR) was employed in order to observe the formation of poly (amic acid) and the conversion of poly (amic acid) to the polyimide. The FTIR spectrum of both poly (amic acid) and polyimide were given in Figure 6.28.

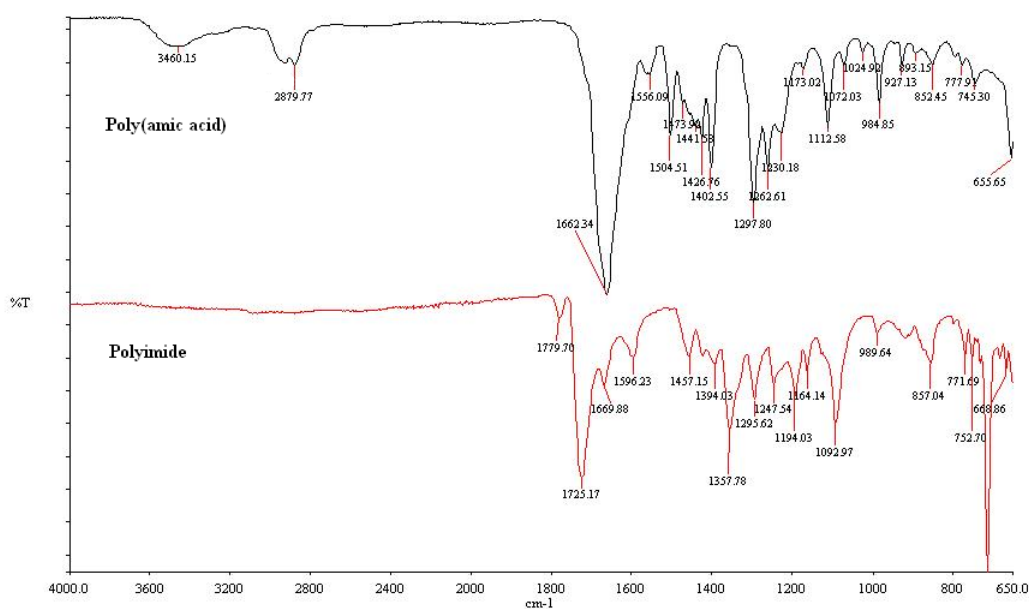


Figure 6.28: FTIR spectrum of poly(amic acid) and polyimide of BTDA-DABA

In poly (amic acid) spectrum, the characteristic absorption bands of acid are observed. While 3460 cm^{-1} indicates amide groups (NH-C), the two bands at 2879 cm^{-1} and 1662 cm^{-1} demonstrates the aliphatic groups and carboxylic groups (–COOH), respectively.

The FTIR spectrum of BTDA-DABA displays several bands associated with its functional groups. The spectrum shows bands at around 1780 cm^{-1} , which is assigned to C=O asymmetric stretch of imide groups, 1724 cm^{-1} that is related with C=O symmetric stretch of imide groups, and 1396 cm^{-1} which is attributed to C–N stretch of imide groups. Peaks at 1092 cm^{-1} and 752 cm^{-1} are from the imide ring bending vibration. The additional band at 1669 cm^{-1} is associated with C=O stretches of benzophenone[59].

Furthermore, it is obvious that all peaks related with poly (amic acid) disappeared in polyimide spectrum. Also the absence of the absorption bands of the amide group at 3460 cm^{-1} indicating that polymer had been completely imidized. FTIR bands of poly(amic) acid and polyimide of BTDA-DABA with respect to their functional groups are presented in Table 6.6.

Table 6.6: FTIR bands of poly(amic) acid and polyimide of BTDA-DABA with respect to their functional groups

Poly(amic acid)		Polyimide	
Absorption bands (cm^{-1})	Functional Group	Absorption bands (cm^{-1})	Functional Group
3460	NH-C	1780	C=O asymmetric stretch of imide
2879	Aliphatic group	1724	C=O symmetric of imide stretch
1662	–COOH	1669	C=O stretch of benzophenone
		1396	C–N stretch of imide
		1092 and 752	Imide ring bending

Molecular weight and polydispersity index of synthesized polyimide were tried to estimate by Gel Permeation Chromatography (GPC) which is relative to polystyrene standards with Tetrahydrofuran (THF) as mobile phase. However it was observed that BTDA-DABA is not soluble in THF therefore the molecular weight value cannot be obtained with available analysis system.

Differential scanning calorimetry (DSC) measurements were conducted using a Perkin-Elmer DSC 4000 calorimeter under nitrogen purge at a heating rate of 20°C/min. In the DSC measurement, two heating cycles were carried out but glass transition of polyimide was observed at the first heating which is up to 350°C. At the second heating polyimide showed no glass transition. It is known that the polyimide chains can be thermally crosslinked after heating treatments at inert medium [18]. Due to the polar groups of DABA, polyimide may thermally crosslinked therefore the PI showed no T_g after second heating process which is up to 400°C.

The DSC thermogram of the first heating process, which is given in Figure 6.29, shows that synthesized BTDA-DABA exhibits a glass transition temperature at 342 °C which was calculated by half- C_p extrapolation. This result agrees well with our simulation result that is 349 °C.

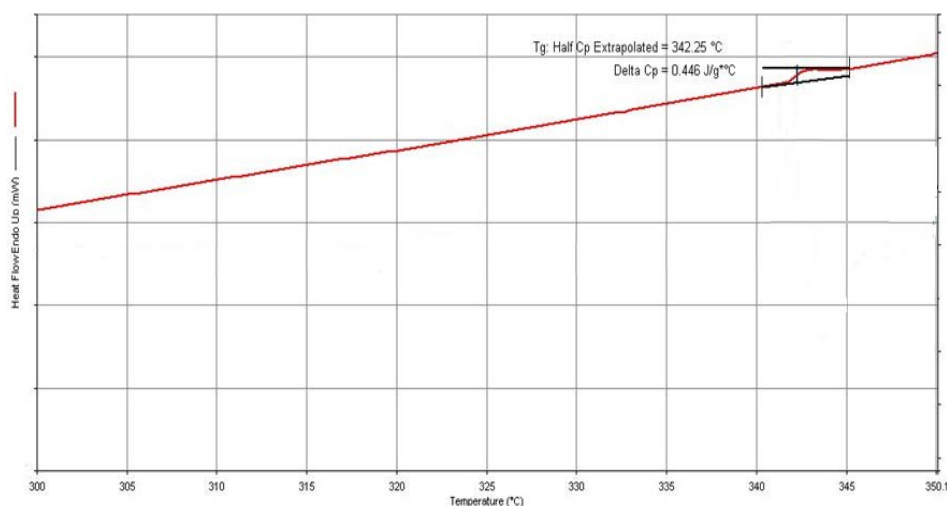


Figure 6.29: DSC thermogram of BTDA-DABA.

Thermal gravimetric analysis (TGA) was done in order to evaluate thermal stability, weight loss, and sample purity of polyimide. Thermogram was collected with 20°C per minute heating rate from 50°C to 550°C in the presence of nitrogen purge.

Weight loss is illustrated as the function of temperature and BTDA-DABA exhibited 4 different weight loss step as shown in Figure 6.30. and Table 6.7.

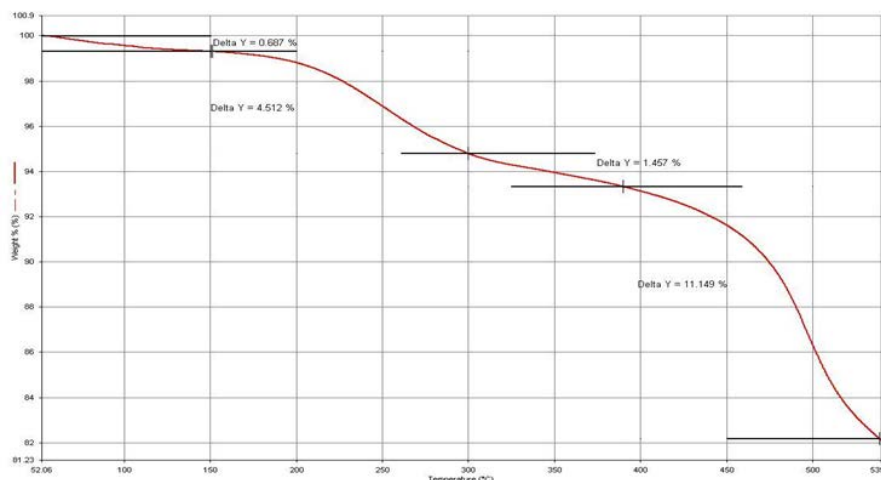


Figure 6.30: TGA thermogram of BTDA-DABA

Due to hygroscopic feature of DABA moiety, weight loss from 50°C to 150°C can be considered as water content of polyimide. NMP and DCB that were used as solvent during synthesis have boiling point at 204°C and 174°C, respectively. The weight loss between 150°C and 300°C is resulted from solvent content of polyimide, after glass transition, chain mobility of polyimide increases so polyimide released all solvent inside its chain between 300°C and 390°C. Finally, thermal degradation of polyimide started at 390°C where polyimide exhibits weight loss about 11%. High degradation temperature indicates that BTDA-DABA is a thermally stable polyimide.

Table 6.7: Weight Loss of BTDA-DABA

Temperature (°C)	Weight Loss (%)
50-150	0.687
150-300	4.512
300-390	1.457
390-550	11.549

Wide-angle X-Ray diffraction (WA-XRD) was used to determine the interchain spacing (d-spacing) in synthesized polyimide. Bragg's equation (Eqn. 4.1) was used

to determine d-spacing value. Two sharp diffraction peaks are observed in XRD pattern of BTDA-DABA as shown in Figure 6.31. These peaks appear at $2\theta = 15$ and 26 which correspond to d-spacing value of 3.60 \AA , and 6.24 \AA , respectively. However, weak diffraction peaks are observed at $2\theta = 10$ and 13 . This situation can be considered as small crystal regions which may formed because of increased solubility of the monomers in the solvent medium during synthesis [60].

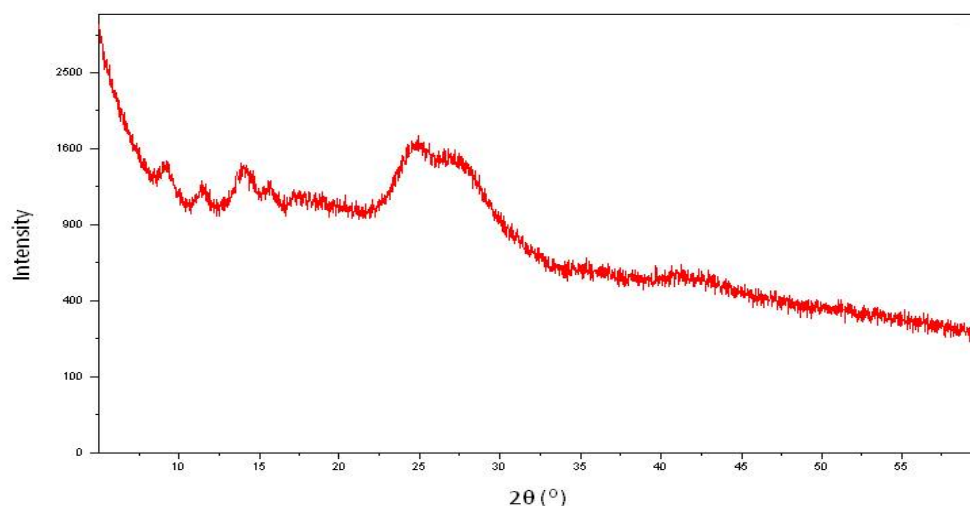


Figure 6.31: X-ray diffraction curve of synthesized BTDA-DABA

Table 6.8 presents glass transition temperatures and d-spacing values that are obtained from experimental and simulation study of BTDA-DABA. The DSC analysis yielded a T_g value of 342°C for the synthesized BTDA-DABA that agrees well with our simulation result which is 349°C . However, there is dissimilarity between results of both studies in comparison with the the experimental values which are reported by Tsuzumi et al [56]. These dissimilarity may be due to difference in procedure of both synthesis and characterization.

Table 6.8: The glass transition temperature and d-spacing values of BTDA-DABA obtained from simulation and experimental study

	Experimental	Simulation	Literature[56]
d-spacing (\AA)	6.24-3.60	6.6-4.8	11.8-7.4
T_g ($^\circ\text{C}$)	342	349	298

7. CONCLUSIONS AND RECOMMENDATIONS

Structural properties and sorption behaviors of 6FDA/BTDA-DABA, 6FDA-DABA and BTDA-DABA have been estimated using molecular simulation tools in order to develop the relationship among the structural properties and structure-solubility relationship of the polyimides and the corresponding copolyimide. All simulations were performed using the *Accelrys Materials Studio 4.1* and *5.1* software packages and molecular interactions were modeled using the COMPASS forcefield. Random configurations of 6FDA-DABA, BTDA-DABA and 6FDA/BTDA-DABA matrices were generated, and characteristic properties such as glass transition temperature (T_g), d-spacing value, cohesive energy density (CED), radius of gyration (R_g), fractional free volume (FFV), accessible free volume (AFV), and the distribution of dihedral angle of the dianhydride and diamine linkage and bridging groups of polyimide matrices were estimated. Finally solubility coefficients and solubility selectivities of sorbate molecules and radial distribution function analyses of CO_2 molecules were determined.

BTDA-DABA has the lowest d-spacing value than 6FDA-DABA and 6FDA/BTDA-DABA. The latter two exhibit similar x-ray patterns with the d-spacing value of 6FDA/BTDA-DABA being between the corresponding values of its polyimides.

FFV, CED and R_g values of BTDA-DABA are greater than 6FDA-DABA and 6FDA/BTDA-DABA. All these values of 6FDA/BTDA-DABA are between the corresponding values of its polyimides.

T_g of polyimides are close to each other but BTDA-DABA has higher glass transition temperature than 6FDA-DABA. The torsion angle distribution of the carbonyl bridge of BTDA is narrower that confirms rigidity of carbonyl-bridge of BTDA with respect to hexafluoroisopropylidene bridge of 6FDA. The linkage between amino groups of dianhydrides and diamine of polyimide and copolyimide matrices are identical therefore the torsion angle distributions of the linkage are almost same. The higher T_g value of BTDA-DABA indicates that the backbone

rotation of BTDA-DABA is restricted therefore it creates more free volume thus FFV of BTDA-DABA is higher than 6FDA-DABA.

Compared to its corresponding polyimides 6FDA/BTDA-DABA exhibits glass transition unexpectedly at a higher temperature because both carbonyl and hexafluoroisopropylidene bridges restrict the rotation of copolyimide.

In agreement with aforementioned properties, higher CED and R_g values show that BTDA-DABA packed closely than others, therefore interchain spacing (d-spacing) of BTDA-DABA is the lowest.

Structural properties of 6FDA-DABA are in good agreement with the data available in the literature. T_g and d-spacing values of BTDA-DABA that were obtained from our experimental study are close to that estimated from molecular simulation technique however there is a discrepancy with respect to values reported in the literature.

Sorption behaviors of O_2 , N_2 , CO_2 and CH_4 in polyimides and copolyimide are similar but solubility of these gases in BTDA-DABA is the highest. For mixed gas case; the selectivity of BTDA-DABA for CO_2/CH_4 mixture is higher than 6FDA-DABA and 6FDA/BTDA-DABA. Solubility coefficients of C_3H_6 and C_3H_8 in 6FDA/BTDA-DABA are higher than its polyimides.

Radial distribution function analyses indicate that stronger interactions between polyimides and gas molecules lead to volume dilatation and plasticization, which increase accessible free volume of the polyimide matrices to accommodate sorbate molecules. Simulations of plasticization induced by CO_2 , C_3H_6 and C_3H_8 shows that the swelling of 6FDA/BTDA-DABA is more significant than its corresponding polyimides. 6FDA-DABA is the most resistant polyimide to plasticization.

The investigation of structural properties and structure-solubility relationship in the polyimide membranes by an atomistic level simulation is essential to develop high performance polymeric membranes for gas separation applications. Therefore, in order to predict permeabilities of O_2 , N_2 , CH_4 , CO_2 , C_3H_6 and C_3H_8 in 6FDA-DABA, BTDA-DABA and 6FDA/BTDA-DABA matrices, diffusion coefficients of these gases should be estimated in the future work. Furthermore, in order to estimate molecular weight and polydispersity index of synthesized BTDA-DABA, solubility

tests of the polyimide should be carried out, and Gel Permeation Chromatography (GPC) analysis should be performed with an elution solvent in which the polyimide is soluble. Moreover the synthesis and the characterization of 6FDA/BTDA-DABA should be performed.

REFERENCES

- [1] **Yampolskii, Y., and Freeman, B.**, 2010: Membrane Gas Separation. John Wiley&Sons Ltd., United Kingdom.
- [2] **Robeson, L.M.**, 1991: Correlation of separation factor versus permeability for polymeric membranes. *Journal of Membrane Science*, **62**, 165-185
- [3] **Robeson, L.M.**, 2008: The upper bound revisited. *Journal of Membrane Science*, **320**, 390-400.
- [4] **Halitoğlu S., Tanteekin-Ersolmaz Ş.B.**, 2007. Prediction of gas permeability coefficients of copolyimides by group contribution methods, presented at the NAMS meeting, May 12-16, 2007, Orlando, Florida.
- [5] **Baker R. W.** 2004: Membrane Technology and Applications, John Wiley & Sons, Ltd, Menlo Park, California.
- [6] <http://www.co2crc.com.au/images/> accessed on May 2nd, 2011.
- [7] **Soltanieh, M., and Gill, W., N.**, 1981: Review of Reverse Osmosis Membranes and Transport Models, *Chemical Engineering Communications*, **12**, 279
- [8] **Stannett V.**, 1978: The Transport of Gases in Synthetic Polymeric Membranes-an Historic Perspective. *Journal of Membrane Science*, **3**, 97.
- [9] **Dhingra S.S.**, 1997: *Mixed Gas Transport Study Through Polymeric Membranes: A Novel Technique*. PhD Thesis, Virginia Polytechnic Institute and State University, Virginia, USA.
- [10] **Haruhiko, O., Kudryavtsev, V.V.**, 1996: Polyimide membranes : applications, fabrications, and properties. Gordon and Breach, Amsterdam.
- [11] **Park, J.Y., Paul, D.R.**, 1997: Correlation and prediction of gas permeability in glassy polymer membrane materials via a modified free volume based group contribution method. *Journal of Membrane Science*, **125**, 23-39.
- [12] **Kesting R. E., and Fritzsche A. K.**, 1993: Polymeric Gas Separation Membranes, John Wiley & Sons, Inc.
- [13] **Yoshiharu, T.**, 2003: Gas sorption and permeation of glassy polymer with microvoids. *Progress in Polymer Science*, **28**, 1377-1401.
- [14] **Paul, D.R., Koros, W.J.**, 1976: Effect of partially immobilizing sorption on permeability and the diffusion time lag. *Journal of Polymer Science Polymer*, **14**, 675-85.
- [15] **Koros, W.J., Paul, D.R., Rocha, A.A.**, 1976: Carbon dioxide sorption and transport in polycarbonate. *Journal of Polymer Science Polymer Physics*, **14**, 687-702.

- [16] **Sanders, E. S., 1988:** Penetrant-induced plasticization and gas permeation in glassy polymers. *Journal of Membrane Science*, **37**, 63-80.
- [17] **Ismail, A.F., Lorna, W., 2002:** Penetrant-induced plasticization phenomenon in glassy polymers for gas separation membrane. *Separation and Purification Technology*, **27**, 173-194.
- [18] **Bos, A., Pünt, I.G.M., Wessling, M., Strathmann, H., 1998:** Plasticization-resistant glassy polyimide membranes for CO₂/CH₄ separations. *Separation and Purification Technology*, **14**, 27-39.
- [19] **Stern, S. A., Saxena V., 1980:** Concentration-dependent transport of gases and vapors in glassy polymers, *Journal of Membrane Science.*, **7**, 47-59.
- [20] **Mauze, G. R. Stern S. A., 1982:** The solution and transport of water vapor in polyacrylonitrile: A re-examination, *Journal of Membrane Science*, **12**, 51-64.
- [21] **Zhou, S., Stern, S. A., 1989:** The effect of plasticization on the transport of gases in and through glassy polymers, *Journal of Polymer Science Part B: Polymer. Physics*, **27**, 205.
- [22] **Wang L., Chang P.X., Cheng C.L., 2006:** Structural Effects of Pendant Groups on Thermal and Electrical Properties of Polyimides. *Journal of Applied Polymer Science*, **100**, 4672–4678
- [23] **Park S.H., Kim K.J., So W.W, Moon S.J., and Lee S.B., 2003:** Gas Separation Properties of 6FDA-Based Polyimide Membranes with a Polar Group. *Macromolecular Research*, **11**, 157-162.
- [24] **Shimazu A., Miyazaki T., Maeda M., Ikeda K., 2000:** Relationships between the Chemical Structures and the Solubility, Diffusivity, and Permselectivity of Propylene and Propane in 6FDA-Based Polyimides. *Journal of Polymer Science: Part B: Polymer Physics*, **38**, 2525-2536.
- [25] **Zhang L., Xiao Y., Chung T.S., Jiang J., 2010:** Mechanistic Understanding of CO₂-Induced Plasticization of A Polyimide Membrane: A Combination of Experiment and Simulation Study. *Polymer*, **51**, 4439-4447.
- [26] **Kang J.W., Choia K., Joa W.H., and Hsub S.L., 1998:** Structure–property relationships of polyimides: a molecular simulation approach. *Polymer*, **39**, 7079-7087.
- [27] **Mayo S. L., Olafson B. D. and Goddard W. A., 1990:** DREIDING: A generic force field for molecular simulation, *Journal of Physical Chemistry*, **94**, 8897-8909.
- [28] **Pan R., Liu X., Zhang A., Gu Y., 2007:** Molecular simulation on structure–property relationship of polyimides with methylene spacing groups in biphenyl side chain. *Computational Materials Science*, **39**, 887–895
- [29] **Liang T.N., Xiaozhen Y., Zhang X., 2001.** *Journal of Polymer Science Part B: Polymer Physics*, **39**, 2243–2251.

- [30] **Tuckerman M.E.**, 2010: Statistical Mechanics: Theory and Molecular Simulation. Oxford Graduate Texts, England.
- [31] **Valleau J. P. And Cohen L. K.**, 1980: Primitive model electrolytes. I. Grand canonical Monte Carlo computations. *Journal of Chemical Physics*, **72**, 5935-5941.
- [32] **Pathria R.K, and Paul D.**, 2011: Statistical Mechanics 3rd edition Elsevier Ltd.
- [33] **Comba, P., Hambley, T. W. and Martin, B.**, 2009: Molecular Modeling of Inorganic Compounds. Wiley-Vch, Germany.
- [34] **Höltje, H.D., Sippl, W., Rognan, D. and Folkers, G.**, 2008: Molecular modeling: basic principles and applications, Wiley-Vch, Germany.
- [35] **Rappé, A. K. and Casewit, C. J.**, 1997: Molecular mechanics across chemistry. University Science Books, Sausalita, California.
- [36] **Martin M. G.**, 2006. Comparison of the AMBER, CHARMM, COMPASS, GROMOS, OPLS, TraPPE ve UFF force fields for prediction of vapor–liquid coexistence curves ve liquid densities, *Fluid phase equilibria*, **248**, 50-55.
- [37] **Li T., Kildsing D. O. and Park K.**, 1997: Computer simulation of molecular diffusion in amorphous polymers, *Journal of controlled release*, **48**, 57-66.
- [38] **Katajisto J., Linnolahti M., Haukka M. and Pakkanen T. A.**, 2003: Development of a New Force Field for Property Prediction of Cyclo-Olefin Copolymers, *Journal of Physical Chemistry B*, **108**, 2168-2172.
- [39] **Sun H., Mumby S.J., Maple J. R. and Hagler A. T.**, 1994: An ab initio CFF93 all atom force field for polycarbonates, *Journal of the American Chemical Society*, **116**, 2978-2987.
- [40] **Sun H.**, 1998: COMPASS: An ab Initio Force-Field Optimized for Condensed-Phase Applications-Overview with Details on Alkane and Benzene Compounds. *J. Phys. Chem. B*, **102**, 7338-7364.
- [41] **Sadus, R. J.**, 2002: Molecular Simulation of Fluids Theory, Algorithms and Object-Oriented. Elsevier, Amsterdam.
- [42] **Sanchez C.**, 2010: *Molecular simulations in microporous materials: adsorption and separation*. Master of Philosophy Thesis, University of Granada, Spain.
- [43] **Ungerer, P., Tavitian, B., and Boutin, A.**, 2005: Applications of Molecular Simulation in the Oil and Gas Industry - Monte Carlo Methods. Editions Technip, Paris.
- [44] **Berendsen, H. J. C.; Postma, JPM; Van Gunsteren, WF; Dinola, A; Haak, JR**, 1984: Molecular-Dynamics with Coupling to an External Bath. *Journal of Chemical Physics*, **81**, 3684–3690.
- [45] **Hess B.**, 2007. Force fields, thermo- and barostats, GROMACS workshop 2007.
- [46] **Leach A.R.**, 2010: Molecular Modelling Principles and Applications, 2nd edition, Pearson, Prentice Hall.

- [47] **Frenkel, D., Smit, B.**, 2002: Understanding Molecular Simulation From Algorithms to Applications. Academic Press, San Diego.
- [48] **Wind J.D., Staudt-Bickel C., Paul D.R. and Koros W.J.**, 2002: The Effects of Crosslinking Chemistry on CO₂ Plasticization of Polyimide Gas Separation Membranes. *Ind. Eng. Chem. Res.*, **41**, 6139-6148.
- [49] **Xua W., Paul D.R., Koros W.J.**, 2003: Carboxylic acid containing polyimides for pervaporation separations of toluene/iso-octane mixtures. *Journal of Membrane Science*, **219**, 89-102.
- [50] **Fang X., Wang Z., Yang Z., Gao L., Li Q., Ding M.**, 2003: Novel polyimides derived from 2,3,30,40-benzophenonetetracarboxylic dianhydride. *Polymer*, **44**, 2641–2646.
- [51] **Heuchel M., Hofmann D., and Pullumbi P.**, 2004: Molecular Modeling of Small-Molecule Permeation in Polyimides and Its Correlation to Free-Volume Distributions. *Macromolecules*, **37**, 201-214.
- [52] **Carraher E. C. Jr.**, 2007: Seymour/Carraher's Polymer Chemistry, 7th Edition, CRC Press, USA.
- [53] **Park, H.B., Kim, Y.K, Lee, J.M., Lee, S.Y., Lee, Y.M.**, 2004: Relationship between chemical structure of aromatic polyimides and gas permeation properties of their carbon molecular sieve membranes. *Journal of Membrane Science*, **229**, 117-127.
- [54] **Wind J. D.**, 2002: *Improving Polyimide Membrane Resistance to Carbon Dioxide Plasticization in Natural Gas Separations*, PhD Thesis, The University of Texas at Austin, USA.
- [55] **Cornelius C.J.**, 2000: *Physical and Gas Permeation Properties of a Series of Novel Hybrid Inorganic-Organic Composites Based on a Synthesized Fluorinated Polyimide*. PhD Thesis, Virginia Polytechnic Institute and State University, Virginia, USA.
- [56] **Tsuzumi H., Toi K., Ito T., Kasai T.**, 1996: Relationship Between Thermal Properties and Diffusion Coefficients of Gases for Polyimide Films. 1997 John Wiley & Sons, Inc. CCC 0021-8995/97/020389-09.
- [57] **Xiaoa Y., Lowa B.T., Hosseinia S.S., Chunga T.S., Paul D.R.**, 2009: The strategies of molecular architecture and modification of polyimide-based membranes for CO₂ removal from natural gas—A review. *Progress in Polymer Science*, **34**, 561–580.
- [58] <http://pages.uoregon.edu/struct/courseware/> accessed on March 28th, 2011.
- [59] **García M.G., Marchese J., Ochoa N.A.**, 2010: Aliphatic-aromatic polyimide blends for H₂ separation. *International Journal of Hydrogen Energy*, **35**, 8983-8992.
- [60] **Ratta V.**, 1999: *Crystallization, Morphology, Thermal Stability and Adhesive Properties of Novel High Performance Semicrystalline Polyimides*. PhD Thesis, Virginia Polytechnic Institute and State University, Virginia, USA.

APPENDIX. Sorption behaviors of CO₂, C₃H₆, C₃H₈, CO₂/CH₄ and C₃H₆/C₃H₈ in BTDA-DABA and 6FDA/BTDA-DABA matrices.

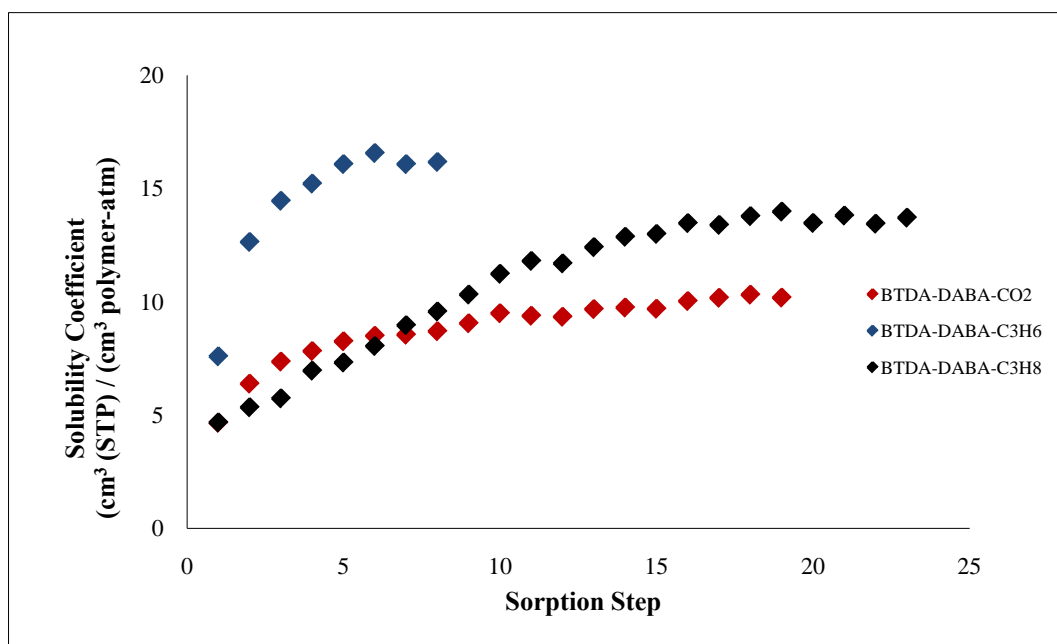


Figure A.1: CO₂, propylene and propane sorption in BTDA-DABA.

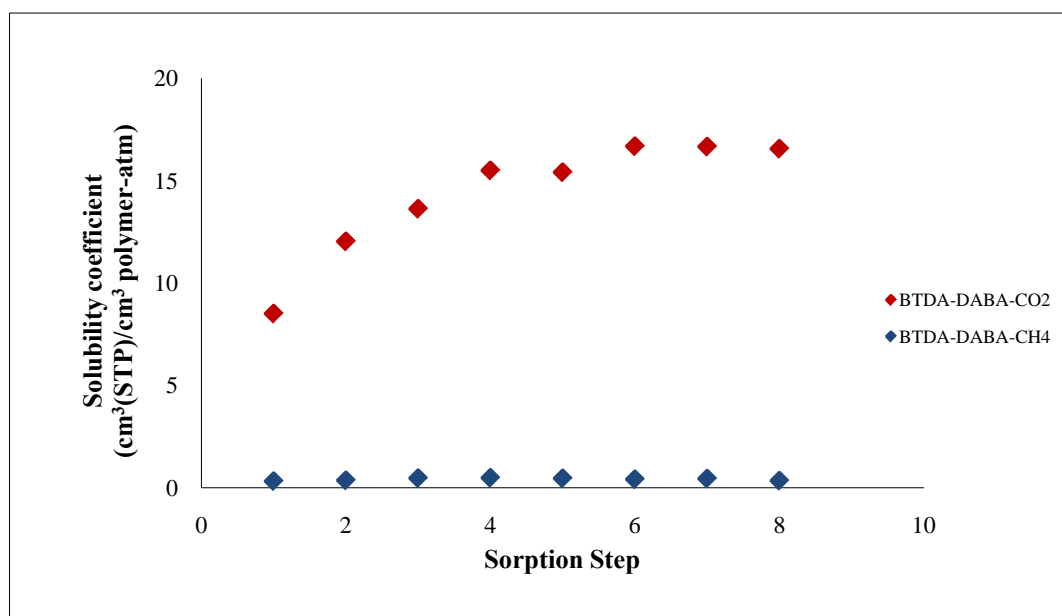


Figure A.2: CO₂/CH₄ sorption in BTDA-DABA.

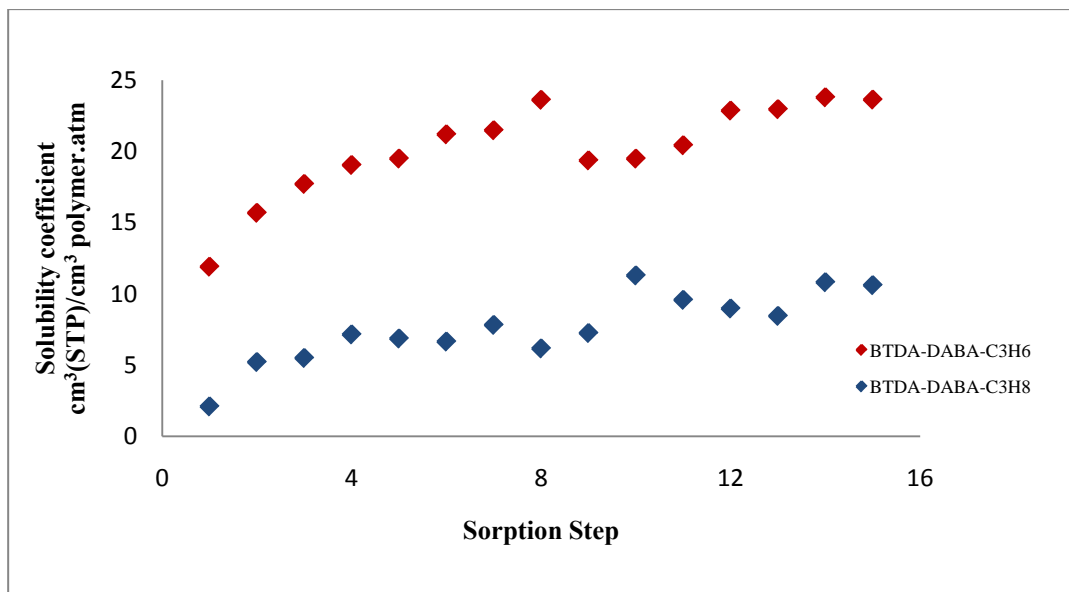


Figure A.3: C₃H₆/ C₃H₈ sorption in BTDA-DABA.

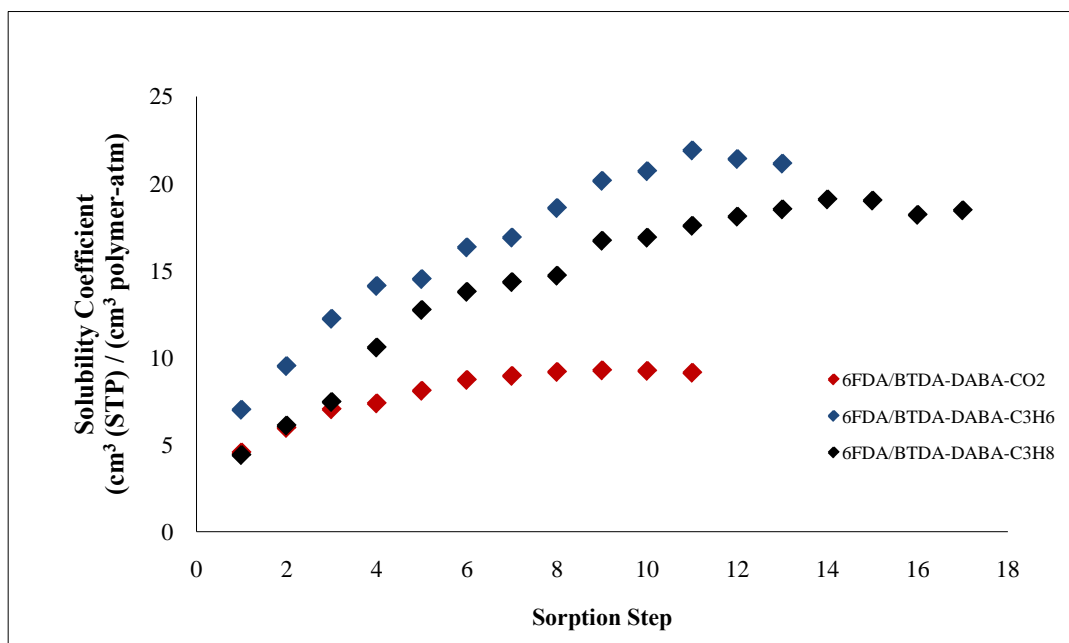


Figure A.4: CO₂, propylene and propane sorption in 6FDA/BTDA-DABA.

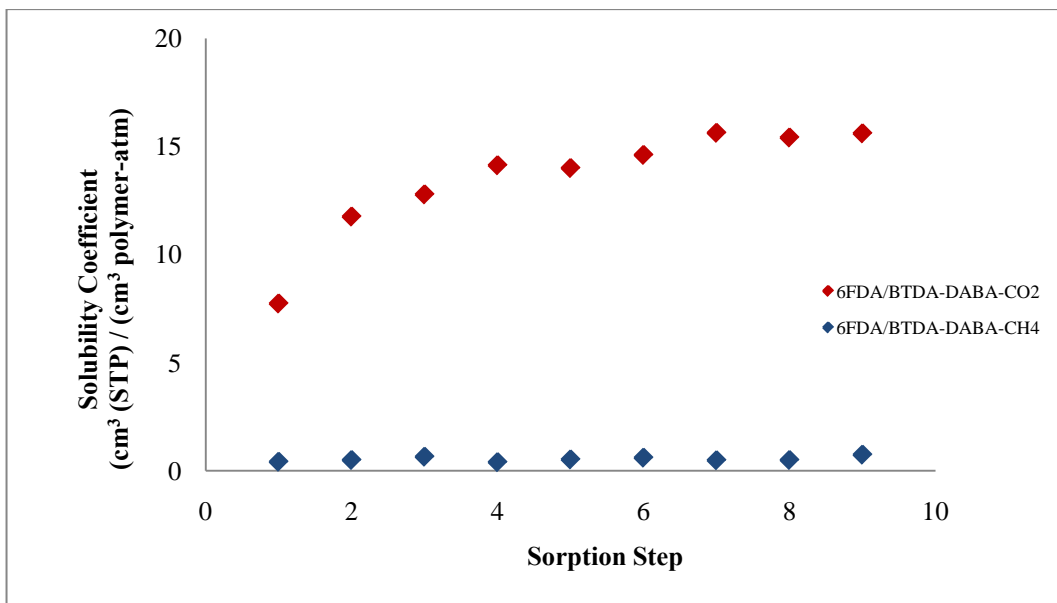


Figure A.5: CO₂/CH₄ sorption in 6FDA/BTDA-DABA.

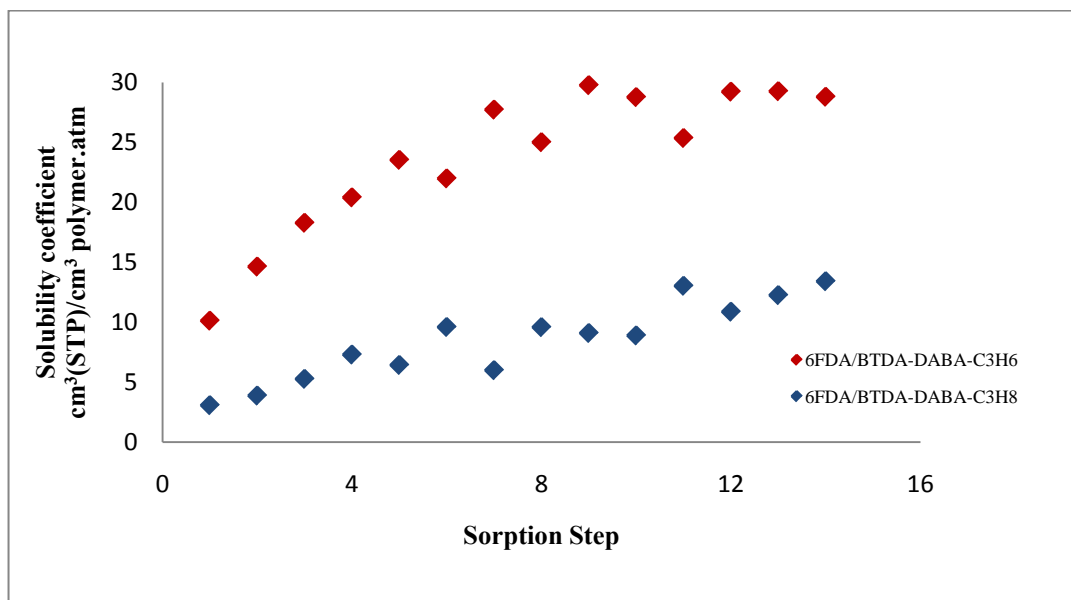


Figure A.6: C₃H₆/C₃H₈ sorption in 6FDA/BTDA-DABA.

CURRICULUM VITAE

Candidate's full name : Işıl KABACAOĞLU

Place and date of birth: Van 02/04/1984

**Universities and
Colleges attended** : B.S.: Chemical Engineering, İzmir Institute of
Technology (2003-2008)
M.S.: Chemical Engineering, İstanbul Technical
University (2009-2011)